
Article:
Actis, P orcid.org/0000-0002-7146-1854 and Leach, AR (2020) Single-Entity Electrochemistry at Confined Sensing Interfaces. Science China Chemistry, 63 (5). pp. 589-618. ISSN 1674-7291

https://doi.org/10.1007/s11426-020-9716-2

SCIENCE CHINA
Chemistry

• REVIEW •

January 2016 Vol.59 No.1: 1–2
doi:

Single-Entity Electrochemistry at Confined Sensing Interfaces

Yi-Lun Ying[1†], Jiajun Wang[1†], Anna Rose Leach[2†], Ying Jiang[4†], Rui Gao[6†], Cong Xu[3,5], Martin A. Edwards[6], Andrew D. Pendergast[7], Hang Ren[8], Connor K. Terry Weatherly[6], Wei Wang[1*], Paolo Actis[2*], Lanqun Mao[3,5*], Henry S. White[6*], Yi-Tao Long[1*]

[1] *State Key Laboratory of Analytical Chemistry for Life Science, School of Chemistry and Chemical Engineering, Nanjing University, 210023, Nanjing, China.*
[2] *School of Electronic and Electrical Engineering, University of Leeds, Woodhouse Lane, LS2 9JT, Leeds (UK)*
[3] *Beijing National Laboratory for Molecular Sciences, Key Laboratory of Analytical Chemistry for Living Biosystems, Institute of Chemistry, the Chinese Academy of Sciences (CAS), Beijing 100190, China*
[4] *College of Chemistry, Beijing Normal University, Beijing 100875, China*
[5] *University of CAS, Beijing 100049, China*
[6] *Department of Chemistry, University of Utah, Salt Lake City, UT 84112, United States*
[7] *Department of Chemistry, The University of North Carolina at Chapel Hill, Chapel Hill, North Carolina 27599, United States*
[8] *Department of Chemistry & Biochemistry, Miami University, Oxford, OH 45056, United States*
[†] *These authors contribute equally to this work*

Received XXXX; accepted XXXX; published online XXXX

Measurements at the single-entity level provide more precise diagnosis and understanding of basic biological and chemical processes. Recent advances in the chemical measurement provide a means for ultra-sensitive analysis. Confining the single analyte and electrons near the sensing interface can greatly enhance the sensitivity and selectivity. In this review, we summarize the recent progress in single-entity electrochemistry of single molecules, single particles, single cells and even brain analysis. The benefits of confining these entities to a compatible size sensing interface are exemplified. Finally, the opportunities and challenges of single entity electrochemistry are addressed.

Single entity, Electrochemistry, Confining effect, Sensors, Nanopores, Nanoparticles, Single cell, Brain

Citation: xxxx

1 Introduction

Why do we need to develop single entity electrochemical measurements? Because the precision and depth of our understanding of chemical systems are determined by analytical science. In traditional ensemble-based studies (cyclic voltammetry, and coulometry), one often measures the averaged activity of an interface containing millions and even billions of elementary entities (*e.g.*, molecules, nanoparticles or cells). These ensemble measurements are subsequently analyzed to extract some averaged values, to describe one or several chemical features. For instance, the morphology and size of nanoparticles and cells are typically evaluated by electron microscopes. Several energy spectroscopies and elementary analysis techniques are available to determine the chemical composition of the nanoparticle/cell. Although powerful, these ensemble-based approaches rely on averaged activities and averaged structural/conformation features, which dilute the intrinsic heterogeneity and blur structure-activity relationships (SAR).[1-4]). Therefore, advancements in under-

*Corresponding authors email: wei.wang@nju.edu.cn (W. Wang); P.Actis@leeds.ac.uk (P. Actis); lqmao@iccas.ac.cn (L. Mao); white@chem.utah.edu (H. S. White); yitaolong@nju.edu.cn (Y.-T. Long)

standing elemental chemical processes and complex chemical reactions is significantly hindered by examining ensembles of entities.

The characterization of individual molecules in bulk solution could help identify rare subpopulations, hidden intermediates, dynamic interactions and multiple reaction pathways.[5] Monitoring single biomolecules deepens the knowledge of fundamental biochemical reaction processes and facilitates precise diagnosis of early-stage diseases. [1, 3, 6, 7] The evaluation of electroactive nanomaterials at single particle level could help to explore the intrinsic heterogeneity of the nanomaterials in terms of both structure and activity.[2, 8, 9] [10] Since the size, morphology, chemical composition, facet, crystallinity, defect and surface chemistry are dramatically different from one nanoparticle to another, the electrochemical activities of individual entities could vary by orders of magnitudes. Single nanoparticle measurements have found numerous applications in broad fields such as batteries, fuel cells and sensors.[7, 11, 12] The investigation of a single cell allows one to explore intracellular and intercellular biochemical process and to uncover the fundamental differences that exist between cells.[13] It provides techniques that could be used for better understanding cellular networks and even tissue function. Regarding the measurement of single tissues, the brain is the most sophisticated organ to be explored. Determining the molecular processes that underpin the development, function, and pathology of the nervous system, however, can be very challenging. [14]

How can one clearly "see" entities, one-by-one, in the bulk? Electrochemistry is a sensitive methodology which converts the characteristics of single entities into the rapid electrochemical response (Figure 1). The electrochemical signature signals refer directly to the single analyte properties such as redox properties, structure, charges and sizes. Compared to the conventional optical microscopy, for instance, which has a detect limitation of ca. 200 nm,[15] the electrochemical approach with nanoscale sensing interface could feasibly achieve nanometer scaled spatial resolution.[2] Moreover, energy spectroscopy usually requires ultra-high vacuum conditions, but provides relatively low temporal resolution.[16] However, the development of electrochemical instrumentation has provided us with ultra-high temporal resolution with high current sensitivity, approaching femtoampere levels.[17] These electrochemical signals contain rich dynamic information from single entities, which could help to understand the fundamental unit of a chemical system.

The main challenges in the electrochemical measurement of single entities is the construction of an appropriate sensing interface. [18, 19] Traditionally, macroscale interfaces report the ensemble features of target analytes. If a micro/nano area is taken from the traditional macroscale sensor, it could then turn into a confined structure for reducing the size of the sensing interface.[20] Then, the size of the sensing interface could be designed to be compatible with sensing a single target entity. The suitable sensing interface could be a single particle, a planar nanosized electrode or a nanochannel. For example, nanometer-sized pore forming biomolecules (nanopores) can provide a well-defined space for accommodating of a single molecule[20, 21] As a single molecule enters a nanopore, it modulates the ionic flux though the pore, resulting in an ionic fluctuation with sub-millisecond temporal resolution and near atomic spatial resolution.[5, 6, 22-29] For detecting single nanoparticles, nanometer sized electrodes and nanopipettes, have been fabricated, which allow detection of one single nanoparticle at a time on its surface. [7, 10-12, 15, 30, 31] Moreover, nanometer sized tips provide high spatial resolution for extracting the content of individual cells as well as for high-resolution imaging of live cells. The micro-sized and chemically engineered electrodes show remarkable advantages in electrochemically determination of neurochemicals in the brain by overcoming the challenges of in vivo selectivity and stability. With an appropriately designed sensing interface, electrochemical approaches offer one of the most sensitive and effective techniques that can be employed to acquire new knowledge of chemical systems.

The term "single-entity electrochemistry" was first coined in 2016 at the Faraday Discussion at York, UK, which brought together scientists from different branches of electrochemistry to discuss diverse approaches and techniques toward similar goals.[1] As mentioned, the single entity interrogated by sensitive electrochemistry requires an adequate sensing interface.[29, 32] For single molecule/nanoparticle analysis, the nano-interface is a necessity. In 2018, the Faraday Discussions themed "Electrochemistry at nano-interface" was held at Bath, UK. There, it was noted that the development of a well-defined nano-scale sensing interface is still a challenge for single-entity electrochemistry. In this review, we summarize the recent progresses and goals of single-entity electrochemistry for analyte scales as small as single molecules, nanoparticles, and cells (Figure 1). Then, we discuss the applications for single-entity electrochemistry to solve the questions from the biological and chemical processes, including measurements performed in the brain and highlight electrochemical methods where precise descriptions of complex electrochemical process are determined with high temporal and spatial resolution. Finally, unmet challenges and future opportunities for the field of single-entity electrochemistry are discussed.

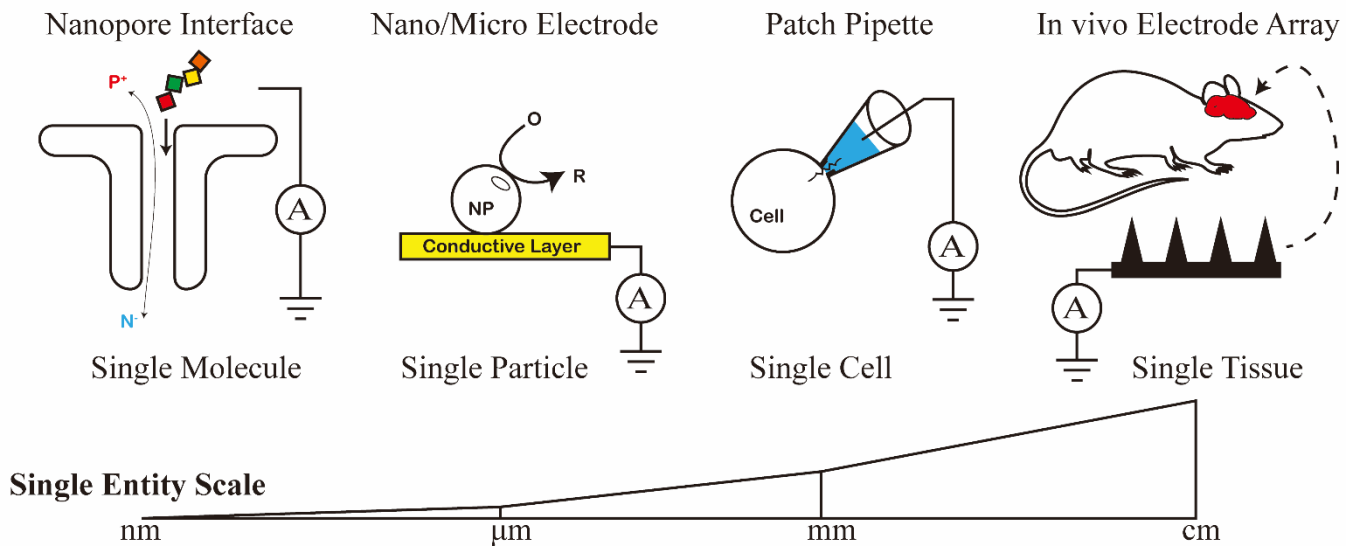

Figure 1 Road map of single entity electrochemistry approaches. The nanopore interface is a water filled pore that allows ions (cation (P^+) and anion (N^-)) bypass. The pore lumen fits the nanometer scale analytes and probe their characteristics. The single nanoparticles (NP) are probed by the nano/micro-scale electrode. Single cell is clamped by nanopipette-based electrochemical measurements. Electrochemical reaction at the cellular surface or intracellular biomolecules is characterized via the electric responses. In vivo analysis of the tissue is performed by the electrode array. By positioning the array at the region of interest, the signal allows to characterize the electrophysiological behaviour.

2. Nanopore-based single molecule analysis

Single molecule sensing requires a compatible sensing interface to provide sufficient amperometric resolution and temporal resolution. Confining a single analyte into a suitable space, assembled by sensing elements and without interference, from neighbor analytes, is the ideal case for single molecule sensing. [5, 29, 33] A nano-scale cavity, nanopore, is an ideal model of such space. By applying a bias voltage, the single analyte together with conducting ions are confined into such an interface that spatially suitable to single molecule allowing label-free detection. To establish a such nanopore, membrane channels are chosen and with careful self-assemble process, the whole sensing interface composed by a single biomolecule is assembled (Figure 2a). The volume of this single biomolecule interface is comparable to the single target molecule. Therefore, a single biomolecule interface captures and identifies one-single-molecule-at-a-time. The proof-of-principle experiment was performed by using alpha-Hemolysin, a toxin secreted from *S. aureus*, probing polynucleotides in 1996.[34]

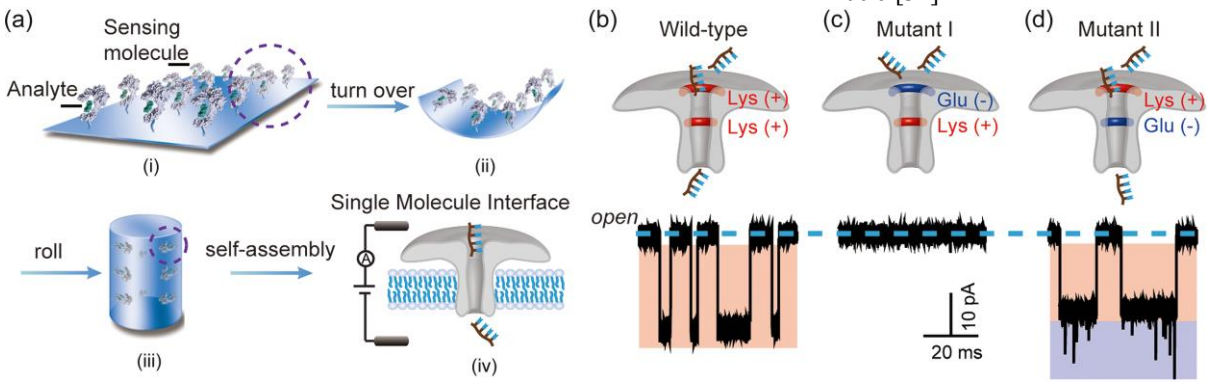

Figure 2 (a) The transformation of a sensing interface. (i) The macroscale interface with a sensing molecule for detection of the targeting analyte. (ii) The macroscale interface shrinks and turns over, (iii) then rolls into a channel as the micro-/nanoscale interface. (iv) A single-biomolecule interface is derived from a single recognition molecule at the nano interface. A self-assembled aerolysin membrane protein is regarded as an example of a single-biomolecule interface. The oligonucleotide is taken as an example for illustrating the analyte. (b) Example of analysing an oligonucleotide through a single aerolysin interface with site-direct mutagenesis. A wild-type aerolysin with two positively charged amino acids produces distinguishable blockage current (red box). The speed of a single negatively charged oligonucleotide translocation aerolysin pore is as slow as ~ 2 ms/base due to the strong electrostatic interactions caused by the positively charged residues at the entrances and inside the lumen. (c) The mutant I with negatively charged glutamic acid located at the entrance of the pore, which generates a high entropic energy barrier for the sensing of negatively charged oligonucleotide molecules. Consequentially, barely no current blockages occur with the continuous time-current recording. (d) The mutant II with negatively charged glutamic acid at the lumen of the single-molecule interface leads to a prolonged duration (red box). The dynamic conformational changes of the oligonucleotide may be enhanced inside the pore due to the electrostatic repulsion, inducing further current oscillations (blue box). Reproduced with permission from [20].

Biosensing in the confined nano-space for single molecule detection has been undergoing for almost 3 decades. The first nanopore themed 'biosensing with channel' workshop was held in Bremen in 2006. The workshop has received international sponsorship since 2011. Since then, the topic of the nanopore gradually altered from understanding to engineering pore-forming materials for broader interests and applications. The Biophysical Society Annual Meeting also lists nanopore as an emerging topic during recent decades. In 2018, a Faraday Discussion collected the research interest themed "electrochemistry at a nano-interface", typically with a section of 'Processes at Nanopores and Bio-Nanointerfaces'. The discussions held in Bath aiming to establish new electrochemical techniques for characterizing dynamic processes at functional nanopores, which are made possible by the integration of novel optical techniques and the development of ultrafast current measurements. Currently, a nanopore-based 4th generation of DNA sequencing tool has been commercialized by Oxford Nanopore Technology (Oxford, UK) and becoming an annually nanopore event on London Calling. The nanopore based single-molecule sensing can currently achieve the sub-microsecond level with sub-picoampere current resolution.

2.1 Construction of the single biological interface (exploring and sensing optimization)

Usually, the nanopore confined space is composed by single biomolecules such as α-Hemolysin,[35] Aerolysin,[36] MspA,[37] OmpG,[38] CsgG,[39] Lysenin,[40] FhuA,[41] YaxAB,[42] phi 29 [43], and BPV E1 helicase nanopore[44] , with some of the examples shown in Figure 3.

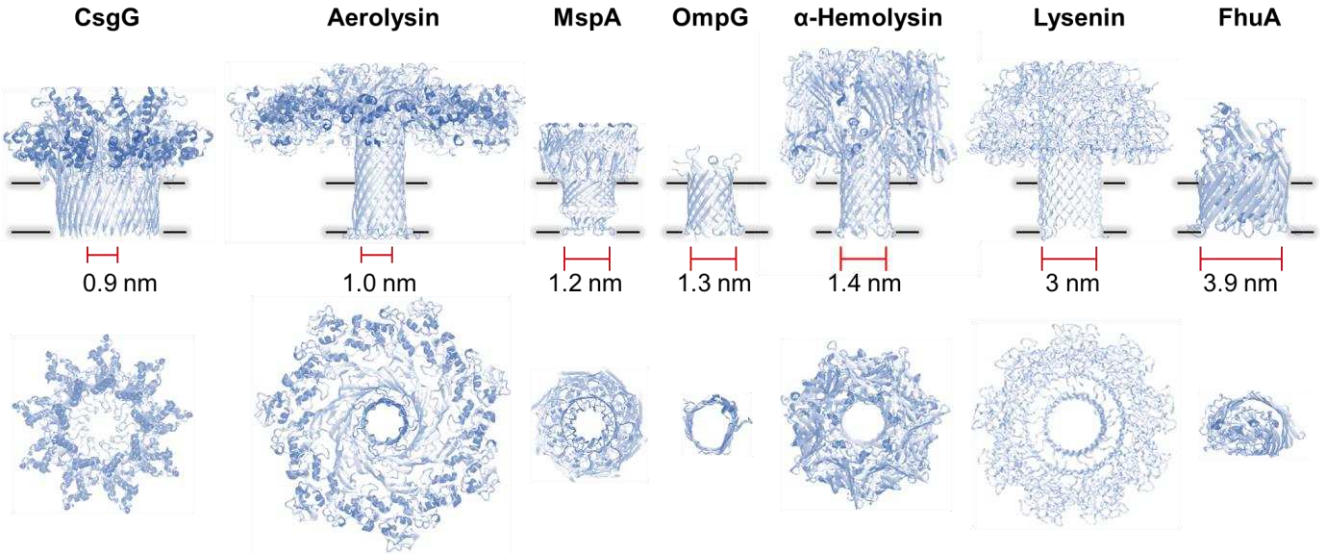

Figure 3 Side and top views of nanopore self-assembled from biological components and the corresponding pore diameter. Narrowest pore opening is indicated in red. The membrane domain where the proteins assemble are hinted by solid lines.

Biological nanopores are natively functionalized in the cellular membrane. In order to take the usage of these biomolecules for the purpose of single molecule probing, an artificial phosphor lipid bilayer is established. Phosphor lipid usually dissolved in the alkane, typically decane for Mueller and Rudin method. Otherwise, the Montel and Mueller method [45] is used to form a solvent-free bilayer. The first approach containing solvent that is more flexible to membrane protein with different thickness of hydrophobic domain, while the latter approach requires a standard pretreatment to the bilayer support, and provides the advantage to build asymmetric bilayer. Both approaches can form a free-standing lipid bilayer that sits on an aperture with diameter of 50-100 μm, which is composed from material such as PTFE. The free-standing lipid membrane is also called 'black lipid membrane' (BLM) named as such because the membrane does not reflect light during the thinning out process. [45]

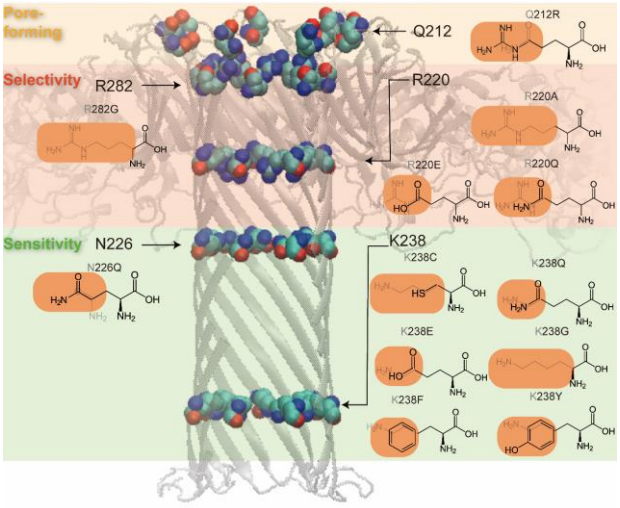

Figure 4 Manipulation of probes at the nanopore based single-biomolecule interface: Possible sites at hot sensing regions of Aerolysin been mutagenized.[46-48]

The self assembly of nanopores from biological material is more sophisticated. Taking Aerolysin nanopore as an example, the aqueous soluble biomolecule undergoes heptamerization, post-prepore, then extends its inner barrel to form a pore with water-filled lumen.[36] During the experimental process, the oligomeric Aerolysin biomolecule is added directly to the BLM forming nanopore with the aid of a membrane bias voltage at negative polarity.[49] The sophisticated membrane protein purification and reconstitution can also be overcome by using native bacterial outer membrane vesicles fusion with artificial lipid bilayer.[50]

The biological nanopore is adjustable in pore diameter with high reproducibility for analytes with difference sizes. Specifically, the introduction of the β-strands increases in pore radii from 1.6 nm for FhuA Δ1-160 up to a maximum of about 2.7 nm for 8 β-sheet insertions. In addition, WT FhuA and its mutants W116S and W112SW116S are mutagenized and obtained the nanopore opening with diameter 1.6 nm, 1.1 nm, 0.84 nm respectively. Aside from the confined effect provided by a nanopore that fits to the analyte at single molecule level, the probing interface can also be precisely manipulated by means of chemical modification as well as biotechnology (Figure 2(b-d)). Figure 4 listed so far engineered Aerolysin, by manipulating the amino acid at the sensing interface, the weak interaction between the probes and analytes is fine tuned for better sensitivity and selectivity. [46-48]

2.2 Nanopore based single-molecule sensing applications

2.2.1 Nanopore for DNA sequencing

Since the completion of human genomic protein in 2003 (https://web.ornl.gov/sci/techresources/Human_Genome/project/index.shtml), DNA sequencing technique are developed in the direction of maximized base per read, cost efficiency and time saving. More importantly, such tool can be used to understand increasingly complexity of phenotypes. [51] The commercialized DNA sequencing tool based on nanopore has shown its great potential. [52] CsgG is engaged with the next generation of ssDNA sequencing[53] and in 2016, the nanopore based DNA sequencer could reach 450 bases per second and enabling 10Gb DNA sequencing data to be obtained. At the current state, further progress is established in length discrimination of oligonucleotide [55] (Figure 5(a)), dsDNA detection [54, 55] (Figure 5 (b)) as well as RNA sequencing[56-58]d (Figure 5 (c)).

2.2.2 Nanopore beyond DNA sequencing

Beyond the sequencing. nanopore based single molecule tool could be used to analyze small molecules, peptides, light driven reaction, chemical reaction, protein folding/unfolding process, enzymology, binding process *etc*. (Figure 5 (e-g)) as discussed below.

Small molecules are difficult to be distinguished with the conventional approaches due to the demand of sub-molecular resolution. The nanopore, towards this hinderance, provides compatible confined space for sensitive electrochemical measurement, resulting molecular resolution and hyper sensitivity. The α-Hemolysin could detect melamine which is a common food additive as low as 10 pM with the aid of DNA probes. [59] Under de novo design by performing mutagenesis, label-free detection is achievable. In the case of monosaccharides, D-glucose and D-fructose exist in aqueous solution as an equilibrium mixture. By controlling the engineered point inside the a-Hemolysin nanopore, a boronic acid reacts reversibly with D-glucose as the pyranose isomer (α-d-glucopyranose) and d-fructose as either the furanose (β-d-fructofuranose) or the pyranose (β-d-fructopyranose). The outcome allows one to discriminate the individual sugar at single molecule level.[60] On the other side, increasing the interaction between the small molecules and sensing interface could

also enhance the discriminate resolution. The K238Q Aerolysin successfully discriminate the cysteine and homocysteine due to the strong interaction provided by the substitution by Glutamine (Q). [61] Azobenzene is a UV-sensitive molecule, by modifying it to the oligonucleotide (Azo-ODN), the cis-to-trans or trans-to-cis modification under the UV-Vis control could be real-time monitored by Aerolysin composed confined space [62] ((Figure 5(e)).

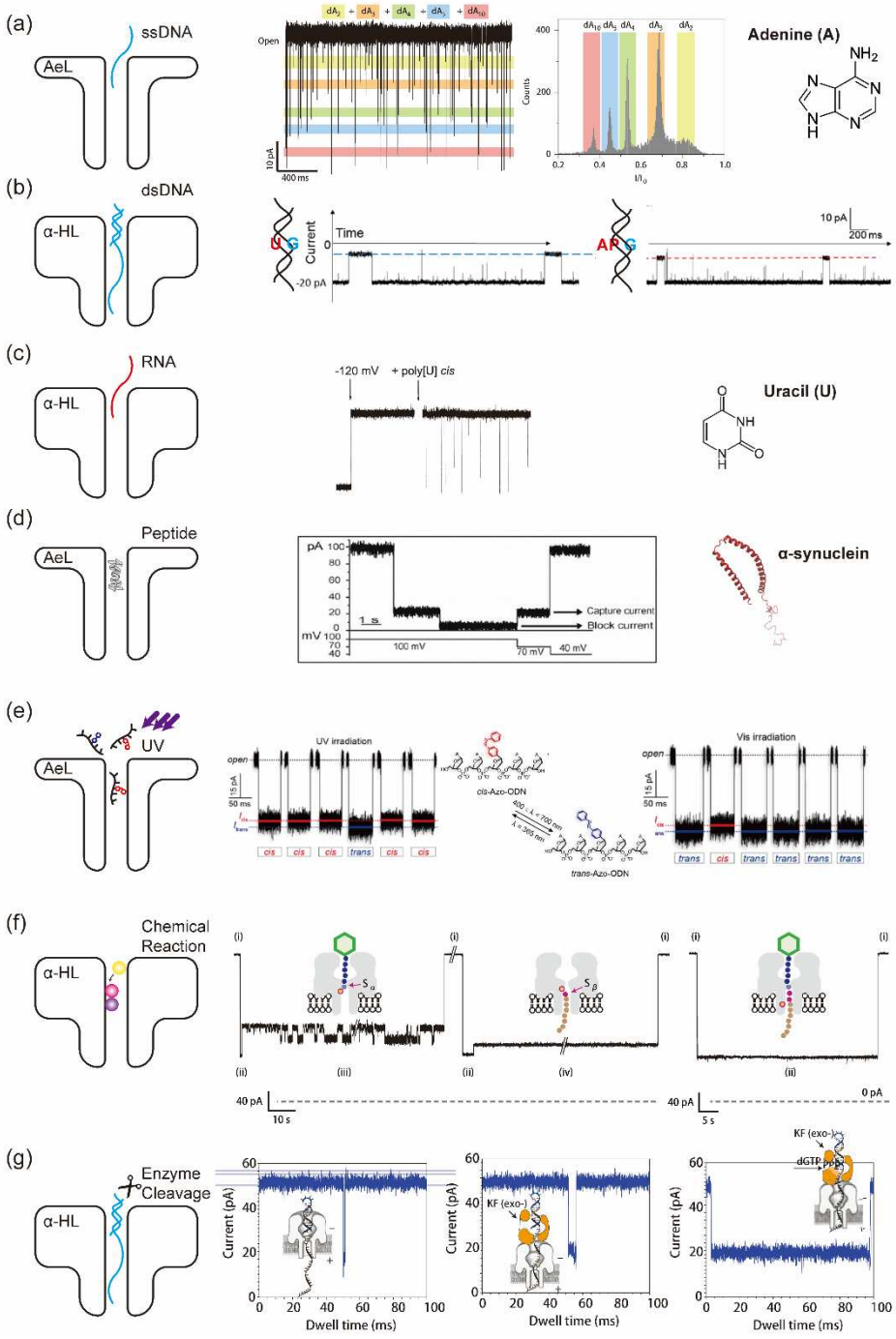

Figure 5 Examples of nanopore based single entity measurements. (a) ssDNA[63] (b) dsDNA[64] (c) RNA[34] (d) Peptide[65] (e) Light driven molecular structure modification[62] (f) Chemical reaction[66] (g) Enzyme cleavage monitoring [67]

Peptides are usually chosen as the biomarkers to diseases. Unlike the DNA segments which are usually negatively charged, the charge density of peptides becomes an important descriptor as well as the 20 amino acid components. The first peptide sequencing by nanopore based electrochemical approach is performed with aHL and Aerolysin.[68, 69] These

works have demonstrated the potential of pore-forming material to detect the peptides and guide the way to design such material for better sensitivity and selectivity. With a prominent example of nanopore sensing disease related peptides, neurodegenerative disorder diseases-related peptides are analyzed by the nanopore label free technique. Alzheimer's disease, Parkinson's disease and the others are associated with the presence and activity of toxic protein aggregates known as amyloids. Common strategies to analyze the biophysical properties of these abnormal aggregation are Ion mobility spectroscopy-mass spectroscopy (IMS-MS), Fluorescence correlation spectroscopy (FSC), cryo-transmission electromicroscopy, Atomic force microscopy and NMR etc., however these techniques provide ensemble information. Nanopore utilized electrochemical signal to analyze the toxic protein aggregates inasmuch the single molecule resolution and label free merits (Figure 5(d)).[27, 70, 71] Specifically, β-amyloid (Aβ) peptides ($A\beta_{25-35}$ and $A\beta_{35-25}$) were distinguished in real-time due to their characteristic blockades. The understanding of the nanopore probing metal-induced folding of peptides or other natural folding states of DNA or peptides at close physiology condition were demonstrated.[27, 72] For instance, the Aβ peptide conformational changes through induced by metal binding (Cu^{2+} and Zn^{2+}) are studied and quantified the binding affinity.[73] Other peptide segments owe similar molecular weight but opposite net charge could be easily distinguished, thanks to the nanopore confined space which enhances the electrostatic interaction between analytes and sensing interface.[74] Homo-peptides with single amino acid difference in length could also be sensitively discriminated by WT Aerolysin nanopore[75] and FraC nanopore.[76]

The chemical reaction process (e.g. cysteine chemistry, phosphorylation etc.) could also be investigated at such biological interface (Figure 5(f)). For example, the disulfate conjugation between analytes and engineered nanopore shows the potential to directional control the molecule movement protensively. [66, 77] The reaction between cysteine and thiol-directed PEG molecule inside the OmpF nanopore could be monitored during the experiment.[77] Rather than the characteristic cysteine chemistry, the click reaction between azide and alkyne at the presence of Cu^{2+} inside a nanopore could also be real-time monitored with label-free merit.[78] The reversible dynamic covalent iminoboronate formation inside the nanopore towards the reactive behavior of the lysine residue located at the pore opening and constriction was studied individually.[79]

During the oligonucleotide moving through the nanopore lumen, single phosphorylation at different positions can be distinguished using Aerolysin by reading out the current stepwise fluctuation.[80] Moreover, distinguish current signature from a-HL could even tell the varients between unphosphorylated, monophosphorylated and diphosphorylated protein ($TrxS112^{-P}$-oligo$(dC)_{30}$).[81] The sensing capability could be optimized by utilizing other nanopore varieties such as CsgG, MspA, aerolysin, FhuA etc. for varies application.

The concept of nanopore based enzymology is addressed.[82, 83] Basically, the enzyme relation biochemical process can be monitored by nanopore based single entity chemistry with provides label-free merits at single molecule resolution (Figure 5(g)). Trypsin is a serine protease which cleaves peptide chains at carboxyl side of the lysine and arginine. The process of Aβ cleavage by trypsin is real time monitored using alpha-Hemolysin by reading the step-wise signature current without labelling. [84] As another case, Exonuclease I is a DNA specific enzyme which catalyzes the removal of nucleotide from linear ssDNA in the 3' to 5' direction. The Aerolysin can monitor the stepwise cleavage of oligonucleotides by exonuclease I (Figure 5 (a)). [63]

Pore forming material is not meant to sense every typical molecule, the probe interface requires *de novo* design. Taking Aerolysin as an example, based on the structural model of such nanopore, the sensing domain for ssDNA translocation has been mapped and demonstrated that R220 and K238 are the critical sensing spots [85]. A series mutants K238C, K238Y, K238F and K238G are then performed and demonstrated that dynamic interaction between analytes and pore interface enhances the better sensitivity for single-molecule analysis (Figure 4). [47] Based on previous results, the weak interaction between the critical sensing spot and the nucleotide is vital to the segment base sensitivity, as a result, the Glutamine is chosen due to the strong interaction with nucleotide bases. As expected, the single lesion nucleotide base in a mixture of heteronucleotide could be discriminated by K238Q.[86] As an another case, the introducing of cysteine in the Aerolysin, K238C, is engineered to monitor the formation of disulphide bond with 5,5′-dithiobis-(2-nitrobenzoic acid) (DTNB) with stepwise resolution owing to formation of disulfate bonds.[87] Furthermore, the precise introduction of cysteine into the α-hemolysin nanopore allows monitoring the individual 0.7 nm steps of a single molecular hopper under the control of electric field.[66] The mutant MspA, M2-NNN MspA, with the aid of phi29 polymerase (DNAP) could control the passage of DNA strand through the nanopore thus boosting the direct distinguish of nucleotide bases.[88] Such mutation along with substrate specified polymerase provides an approach to DNA sequencing. Not only the DNA sequencing, point mutagenesis at E181C of OmpF along with cysteine chemistry allows directional identification of small molecules through the nanopore which is a conundrum for drug screening in nanopores.[89]

3 Single nanoparticle electrochemistry

The challenge here is to resolve the tiny reaction current from single electroactive nanoparticles from the contributions from other individuals as well as the background current (for instance, charging current and polarization current). Because the electrode current itself is blind and has no spatial resolution at all, one has to ensure that there is only one effective

nanoparticle at the electrode surface at the moment of measurement, and to minimize the background current by reducing the size of electrode. Three types of strategies have been proposed to reach this goal as illustrated in Figure 6. In the first strategy (Figure 6(a)), a nanoelectrode was fabricated with an extremely small effective size down to tens of nanometers. A single electroactive nanoparticle with comparable diameter was formed on the nanoelectrode via post-immobilization or *in situ* electrodeposition. Because there was only one nanoparticle and the background current was almost completely suppressed, any electrode current should be attributed to the nanoparticle on the electrode. In the second strategy (Figure 6(b)), a microelectrode was held at an appropriate constant potential to reach a stable and small background current. Very diluted nanoparticle suspension was used to allow for discrete and stochastic collisions of single nanoparticles onto the microelectrode surface, leading to a transient disturbance to the baseline current. The corresponding spike in the current profile was able to reveal the activity of the single nanoparticle in the collision event. The key point of collision strategy is to temporally separate different nanoparticles according to the different times of collision. In the third strategy (Figure 6(c)), a movable nanoelectrode scanned over a substrate surface on which many single nanoparticles had been previously immobilized with a very low number density (coverage). The nanoelectrode-substrate distance was so close that only the individual nanoparticle covered by the nanoelectrode was able to effectively transfer electrons. Consequently, the recorded current can be assigned to a particular individual according to the spatial location of the nanoelectrode. Since this field has been increasing so rapidly, interested readers are referred to these valuable review articles for a comprehensive understanding. [7, 10-12, 15, 31] Here we provide framework descriptions with particular emphasis on the milestones and those most recent studies.

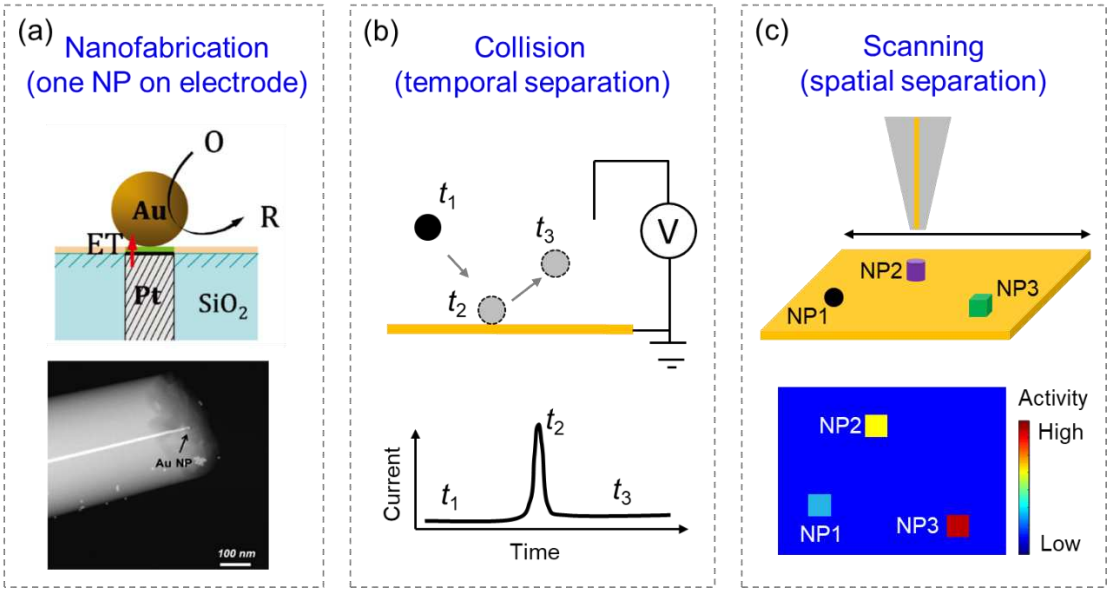

Figure 6 Schematic illustration of three types of strategies for studying single nanoparticle electrochemistry.

3.1 Nanofabrication

The most straightforward solution to study single nanoparticle electrochemistry is to fabricate a nanoelectrode which contains only one nanoparticle on its surface. In order to minimize the background current, it is critical to make sure that the size of nanoelectrode is smaller than, or at least comparable with, that of the nanoparticle. In one of the most earliest attempts, Zhang et al immobilized a single 15-nm gold nanoparticle onto a 10-nm platinum nanoelectrode by virtue of electrostatic adsorption. [90] The successful fabrication was evidenced by transmission electron microscopy characterization, which also revealed the actual size of the nanoparticle (Figure 6(a)). By using oxygen reduction reaction as an example, size-dependent catalytic activity was investigated at single nanoparticle level. [90, 91]

Engineering the nanoparticle-electrode interface plays an essential role here. It must allow for efficient electron transfer between surface-attached nanoparticles and nanoelectrode, and at the same time reach a near-unity surface coverage to suppress the background current. Schuhmann et al recently developed an *in situ* method to synthesize a cobalt-based single metal-organic framework (MOF) nanoparticle on carbon nanoelectrode. [92] The nanoparticle underwent further thermal pyrolysis to produce cobalt-based active sites for oxygen evolution reactions in alkaline solutions. The introduction of single MOF nanoparticle not only provided a well-defined geometry during catalyst preparation, but also helped the characterizations on the amount and distribution of Co-based

catalytic sites.

Because of the heterogeneity, it would be difficult to build a solid SAR by studying only one or a few nanoparticles. Instead, statistical analysis to a sample set containing thousands and even more individuals is usually beneficial to reveal a reliable SAR. In order to achieve this goal, nanofabrication strategy still needs to further improve its efficiency and throughput.

3.2 Single nanoparticle collision

The collision of a single nanoparticle at an ultramicroelectrode disturbs the electrode current. By analyzing such disturbance, the activity of this particular nanoparticle can be evaluated. According to different principles, three types of collision events have been well studied so far, including the blockade mechanism for electrochemically inert nanomaterials, the direct electrochemistry mechanism for redox active nanomaterials, and the catalytic amplification mechanism for electrocatalytic nanomaterials.

In the blockade mechanism, the presence of an electrochemically inert nanoparticle not only reduced the effective surface area of electrode, but also altered the mass transport condition, resulting in the gradual decrease in the current. [93] The current profile carried rich information regarding the property of nanoparticles as well as its interaction with the electrode. For example, if there was a strong attractive force between the nanoparticle and the electrode, a hit-and-stay type collision was expected, accompanying with a staircase decrease in the current profile. In the opposite scenario, no collision can be observed at all if there was a strong repulsion. Under appropriate conditions, hit-and-run type collision can be observed as evidenced by the spike-like negative peaks in the current profile. The residence time (peak width) was an important parameter to explore the nanoparticle-electrode interaction. In addition, statistical analysis on the collision frequency and intensity (peak height or area) has proven powerful to calculate the molar concentration and size of nanomaterials, respectively. Early studies often focused on latex nanobeads and nanodroplets. Increasing attention have been recently paid to biologically significant nanoparticles such as microbials [94] and viruses. [95]

In catalytic amplification mechanism, the collision of an electrocatalytic nanoparticle formed a transient catalytic site to increase the electrode current in the presence of reactants.[96] In addition to the popular metal-based electrocatalyst, an interesting new trend is the photoelectrochemical detection of semiconductor nanoparticles.[97, 98] Under the illumination of light, collision of semiconductor nanoparticles facilitated the charge-carrier separation and increased the photoelectrochemical current in the presence of suitable scavengers.

The colliding nanoparticle itself could undergo electrochemical oxidation or reduction to contribute to the electrode current directly. A typical example was the oxidative stripping of metal nanoparticles such as silver and copper.[99] Because of the extraordinary reactivity of silver nanoparticles, it served as a very popular choice to study the interfacial electron transfer as well as the nanoparticle-electrode interactions. An inversed approach was recently proposed to achieve the reductive synthesis of metal nanoparticles upon the collision of single micelles containing metal salt precursors.[100] In addition to metal nanoparticles, the impact of Li-ion storage metal oxide nanoparticles onto the electrode was also investigated driven by their practical significance in Li-ion batteries.[101] This process involved the intercalation of Li^+ into the nanoparticle. As a modified form of direct electrochemistry, vesicles[102] and liposomes[103] containing redox molecules inside the lipid bilayer membrane could release its cargo upon collision, resulting in the increase in the reaction current.

There are two standing challenges for single nanoparticle collision in SAR studies. First, while the activity of single nanoparticles can be determined from the discrete peaks in the current profile, the structural feature associated with the particular peak is completely missing. Combination of optical microscopes could be a useful development to record the location of collision for further structural characterizations. [101] Second, a constant potential was often applied to the electrode to suppress the charging current. So that this strategy was not quite compatible with the potential sweeping techniques.

3.3 Scanning electrochemical imaging

Scanning electrochemical microscope (SECM) has demonstrated its capability to study single nanoparticle electrochemistry by approaching a nanoelectrode towards a substrate on which nanoparticles were sparsely immobilized. [104] A very promising derivation of SECM is scanning electrochemical cell microscope (SECCM). In this configuration, counter and reference electrodes were placed in a pipette with a tip size of tens of nanometers. When the pipette was filled with solutions and approached to the substrate, a droplet was formed with a contact radius at micrometer scale, which defined the size of effective electrode. When only one surface-immobilized nanoparticle was covered by the droplet, the recorded electrode current could be assigned to this particular nanoparticle. When comparing with nanofabrication approaches, SECCM exhibited significantly improved throughput as the nanopipette can freely hop over the substrate. In a recent report, Unwin and coworkers have shown that the cyclic voltammetry of single $LiMn_2O_4$ nanoparticle can be reliably determined. By virtue of the programmed scanning of nanopipette, the reactivity of hundreds of nanoparticles can be recorded in an one by one manner. [105]

3.4 Optical electrochemical imaging

In addition to these current-based approaches, optical electrochemical imaging represents an alternative and complementary approach to indirectly but quantitatively study single nanoparticle electrochemistry by coupling optical imaging techniques. The basic methodology of optical electrochemical imaging was thoroughly summarized in a recent review article.[15] The brief concept was illustrated in Figure 7. In this configuration, nanoparticles were sparsely immobilized on an optically transparent electrode, such as ITO and ultrathin gold film, which was placed on an inverted optical microscope. With the development of optical imaging techniques, there have been various kinds of optical microscopes that can image single nanoparticles according to the corresponding optical and spectroscopic principles. Optical images of these nanoparticles were continuously recorded to produce a series of time-lapsed images. The optical intensity of each and every nanoparticle was monitored in parallel to report its potential-dependent optical or spectroscopic property. For example, a typical cyclic voltammetry scan to the electrode would lead to the transition between oxidized and reduced states of the nanoparticle, which was indicated by the reversible alternation and recovery of its optical intensity. A suitable optical to electrochemical conversion model was required to quantitatively extract the electron transfer rate, i.e., the current, of single nanoparticles from its optical curve. In order to distinguish from the directly recorded electrode current, one often uses the term, optical current, to describe the indirectly calculated results. Here the potentiostat was solely used to apply the potential and to enable the reactions. The reaction current of single nanoparticles was completely calculated from the optical signals. Recent studies have demonstrated the validity of such conversion by comparing the simultaneously recorded electrochemical current and optical current. [101, 106, 107]

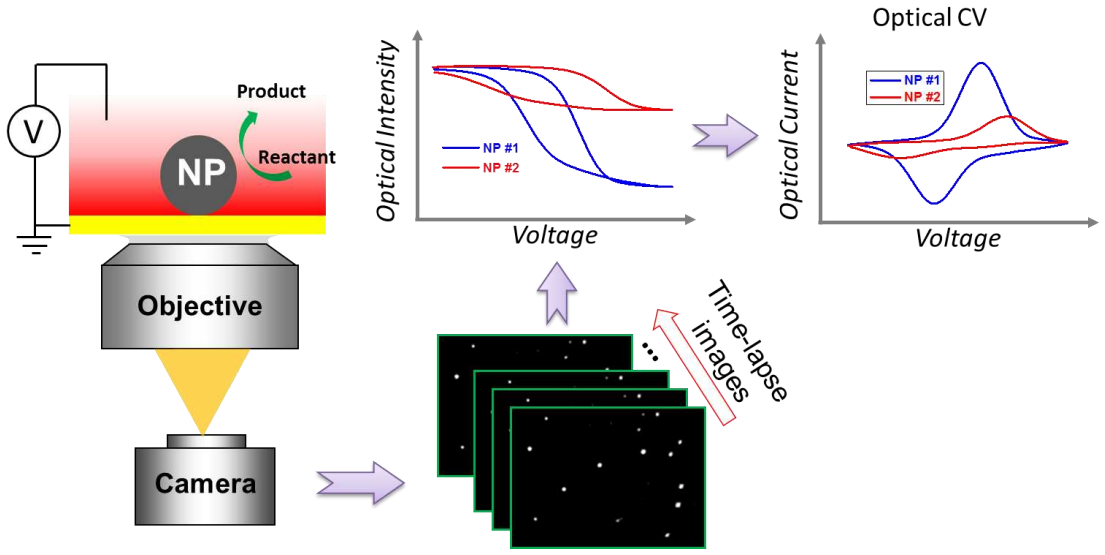

Figure 7 Schematic illustration of the methodology of optical electrochemical imaging

The merit of optical electrochemical imaging relied on the rational design of optical to electrochemical conversion models. As one of the most basic type of optical imaging techniques, bright-field transmission microscope measures the extinction of single nanoparticles. It is therefore sensitive to the absorption spectrum (color). By monitoring the electrochromic kinetics of single tungsten oxide nanorods (a promising material used in smart windows) under bright-field transmission microscope, Sambur and coworkers discovered that a particle-dependent waiting time was required prior to the color change.[108] Dark-field microscope is a powerful format to visualize single plasmonic nanoparticles based on its scattering. It has been demonstrated that the scattering intensity of silver nanoparticles was a function of its volume, and thus the number of silver atoms. According to the dependence, one was able to resolve the reaction rate of single nanoparticles during electrochemically assisted deposition or oxidative stripping.[107, 109-111] Single molecule fluorescence microscopy,[112] Raman microscopy[113] and electrochemiluminescence microscopy[114] were also adopted to evaluate the electrochemical activity of single nanoparticles by detecting the fluorescence, Raman and electrochemiluminescence signals of the product molecules, respectively. Surface plasmon resonance microscopy is a wide-field optical microscopy that is sensitive to the refractive index nearby an ultrathin semi-transparent gold film. The electrocatalytic reduction of protons at a platinum nanoparticle formed hydrogen molecules, which decreased the local refractive index. Tao and coworkers deducted a quantitative relationship to calculate the catalytic current of single nanoparticles out of the optical intensity curves. [115] Wang et al recently discovered the dependence of the refractive index of

single $LiCoO_2$ nanoparticles on its lithiation state during electrochemical cycling, allowing for measuring the optical cyclic voltammogram of single Li-ion storage nanoparticles.[116]

In addition to these Faradaic reactions, non-Faradaic charging of single metal nanoparticles and graphene can also be investigated because the dielectric constant of these materials were dependent on the electron density. The latter can be precisely regulated during electrochemical charging and discharging. Mulvaney et al reported the blue shift of plasmonic band of single gold nanorod when injecting electrons into it by applying a negative potential.[117] The correlation was further utilized to measure the electrochemical impedance spectroscopy of single nanoparticles.[118] The injection of electrons to a graphene monolayer was also found to expand its dimension[119] and to change its optical conductivity.[120] Both effects can be detected by using optical imaging approaches.

4. Single-cell nanosurgery

In a larger scale at mili-meter scale, the cell is the principal, most fundamental unit of life. In 1665, Hooke first used the term 'cell' when observing cork under a microscope. [121] Centuries later, Cell Theory was established by Schleiden, Schwann and Virchow, asserting that cells are the primary structural and functional unit in living organisms, all organisms comprise of one or more cells, and that each cell originates from a pre-existing cell [122]. As the most basic unit of life, cells each carry out their own functions which contribute to the physiology of the organism as a whole, through the expression of genes in each individual cell [123].The common practice of analysing a population of cells in bulk, however, masks the fundamental differences that exist between cells, and only gives us an average picture of what is occurring in healthy and diseased tissues. As result, the investigation of a single cell allows one to explore the intracellular and intercellular biochemical process.

4.1 Single-cell isolation techniques

There are many different techniques available in order to isolate single cells for analysis, the most widely-used approaches being Fluorescence Activated Cell Sorting (FACS). FACS depends on the use of fluorescent makers to label desired cells, and separates cells from a mixed population individually based on their fluorescence. A limitation of FACS is that as it utilises a fluid stream of cells, so that tissue samples need to be dissociated, which could alter their state, and loses contextual information as to where the cells were isolated from. Laser Capture Microdissection (LCM) offers an alternative, where cells from intact tissue are isolated under optical control, retaining spatial information. Although LCM provides spatial context, it does hold its own limitations, a major one being the identification of cells of interest amongst a heterogeneous tissue population, which requires an expert, for example a pathologist. Other disadvantages lie in use of staining agents to visualise the tissue and the use of fixing agents, which can affect downstream analysis, and the LCM excision itself can damage the cell or cellular components. It can also be difficult to isolate the cell of interest on its own, without parts of neighbouring cells. [124] Fluorescence *in-situ* hybridization (FISH), is a technique that employs fluorescently-labelled nucleic acid sequences to dynamically determine the number and location or movement of transcripts within single cells. This technique, however, does not work for all transcripts, and is not able to provide information for as many transcripts at one time as, for example RNA sequencing [125].

Microfluidics has had a monumental role in the progress of single-cell analysis. Microfluidic devices manipulate the movement of liquids within microchannels (on the μm scale), allowing the selective capture of single cells in fluid suspension. These devices can combine isolation of cells with lysis and analysis in a single platform[126]. Microfluidics can be categorised into either valve, droplet or nanowell based approaches, which are all compatible with omics analyses[127].

One caveat to these devices, however, is that they rely on the flow of a suspension of cells, which removes spatial information as to where the cell of interest was isolated from. Recently, Sarkar et al developed a microfluidic device that can overcome this problem by enabling the selective isolation of single cells within a tissue culture. After capture of the cell within its tissue environment, it is lysed and biochemical analysis is performed, in this case enzymatic assays. Such a device could therefore be used to correlate intracellular properties of a cell with its spatial context [128].

As well as having their own unique drawbacks, all of these techniques currently used for single cell analysis, aside from FISH, have the fundamental limitation that they rely on cell lysis, and therefore provide only a 'snapshot' rather than a dynamic analysis of cellular state. There is also a possibility that the lysing buffers themselves could influence intracellular contents. Furthermore, most of these techniques, aside from LCM and Sarkar et al.'s microfluidic chip [128], remove the cell from its natural environment, losing spatial information as to where the cell was isolated.

In order to overcome these shortcomings of single cell analysis approaches, a new field has emerged which employs the use of nanoscale devices to perform 'surgery' on single cells (Figure 8) [129]. Here, instead of being lysed and analysed 'post-mortem', single cells can be sampled from continuously without affecting their viability or removing them from their physiological environment. Cellular contents are extracted at different time points and subsequently analysed, achieving the next level to single cell analysis: spatiotemporal resolution.

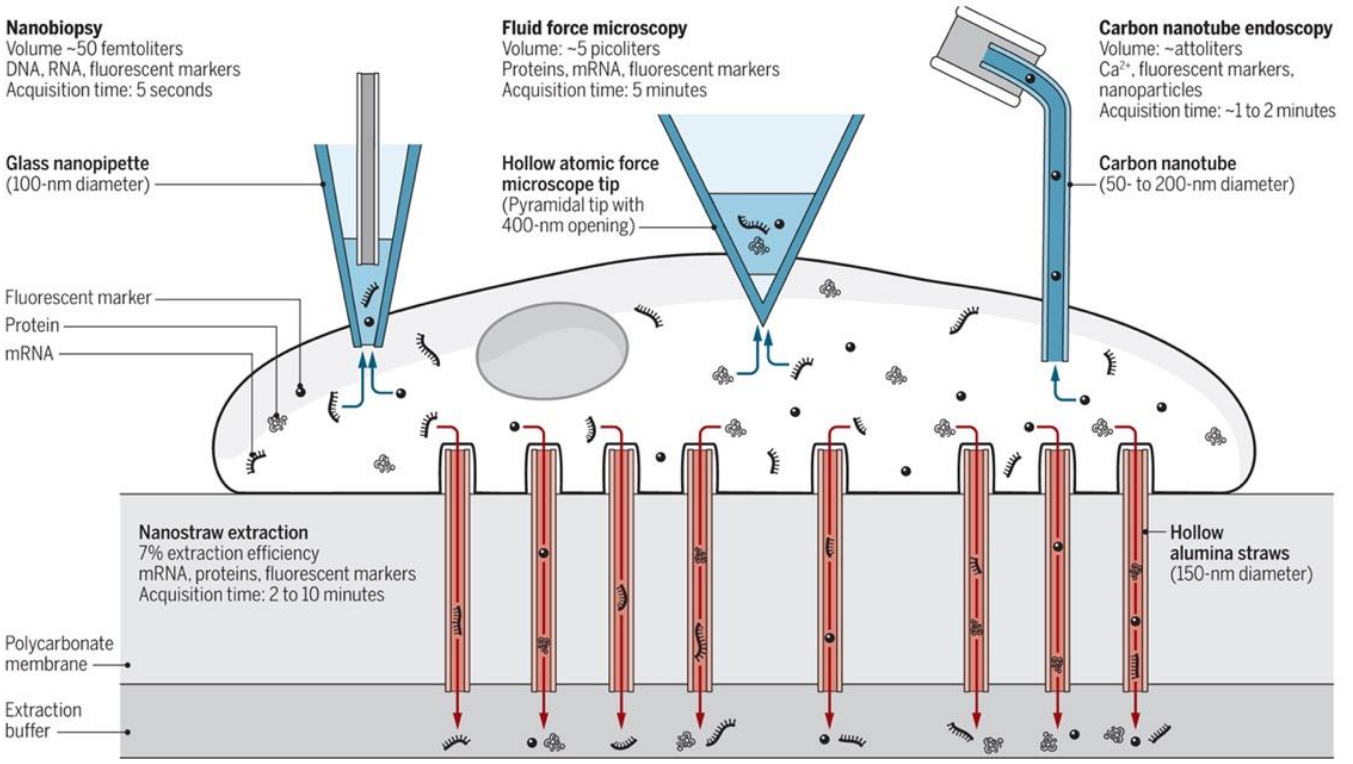

Figure 8 Schematic showing different methods available to extract cell contents. Reproduced with permission from [129]. Copyright 2017, AAAS.

4.2 Dielectrophoretic nanotweezers (DENT)

In 2009, Nawarathna et al. developed a metal-coated Atomic Force Microscopy (AFM) probe capable of extracting mRNA from living cells, which they named the dielectrophoretic nanotweezer (DENT).[130] The authors employed a silicon AFM probe with an insulating SiO_2 layer deposited on top, followed by a Platinum layer. Primers complementary to specific mRNAs were immobilised onto the surface, and the AFM probes were inserted in the cell cytoplasm. The application of an AC voltage between the silicon core and the outer Pt layer generates a dielectrophoretic force which attracts mRNAs present in the cell cytoplasm which then hybridise to the primers on the AFM probes. This technique was used to extract the mRNA of the housekeeping genes β-actin, GADPH and HPRT and the success of the extraction was confirmed by cDNA synthesis followed by real-time PCR, and gel electrophoresis. β-actin mRNA was still detected without the application of the alternating potential, but applying the potential increased the efficiency of collection. The authors have also shown that the procedure has non-detrimental effect of cell viability.

In 2011, the same group demonstrated the extraction of β-actin mRNA using qPCR and gel electrophoresis. They additionally demonstrated they were able to extract an oncogene transcript selectively from cells transfected with the transcript, in a mixture of both transfected and wild-type cells [131]. In a more recent paper, the group employed an AFM silicon probe coated with SiO_2 and a Cr/Au layer. This probe was used to capture DNA molecules in different buffers taking advantage of dielectrophoretic trapping [132].

The group have since demonstrated the integration of the technology with microfluidics. The authors have captured single cells in an enclosed PDMS microwell, and use the DENT to penetrate through the PDMS membrane of the microwell, into the cell, and then employed dielectrophoretic trapping to extract mRNAs [133]. The authors analysed the expression of three housekeeping genes from a single live HeLa cell and quantified their expression levels using RT-qPCR. Furthermore, they were able to analyse the dependency on the efficiency of mRNA extraction upon increasing the magnitude of the voltage, and concluded that higher voltages increase the amount of mRNA extracted, due to higher dielectrophoretic force. Post extraction, the cell viability was found to be around 70% for cells under the application of 1.1 and 1.5 V, but was lower for those whose mRNA was extracted using 1.9 V.

The authors next evaluated the use of the DENT-integrated microfluidic chip for identifying cancer cells amongst blood cells, by using a mixture of breast cancer cells and monocytes. They trapped single cells, and extracted mRNA and detected marker transcripts using RT-qPCR. The results showed an mRNA expression 'fingerprint' for each cell type, enabling their identification, even though the cells were similar in size and visual appearance. These results demonstrate the ability of DENT to selectively extract mRNA for expression analysis, and indicate its potential applications to identify specific cell types, for example in a blood sample.

In 2019, Nadappuram et al reported an adaptation of the dielectrophoretic trapping by employing nanotweezers fabricated from dual-carbon nanoelectrodes [134, 135]. The two nanoelectrodes are placed at the tip of a quartz nanopipette and are separated by a 10-20 nm insulating septum which enables the generation of extremely high electric field gradients ($\nabla|E|^2 \approx 10^{28}$ V^2 m^{-3}) that enables the trapping of individual molecules in physiological conditions. The author demonstrated the extraction of nucleic acid from within living cells and also the extraction of one single mitochondrion from a neuron dendrite (Figure 9).

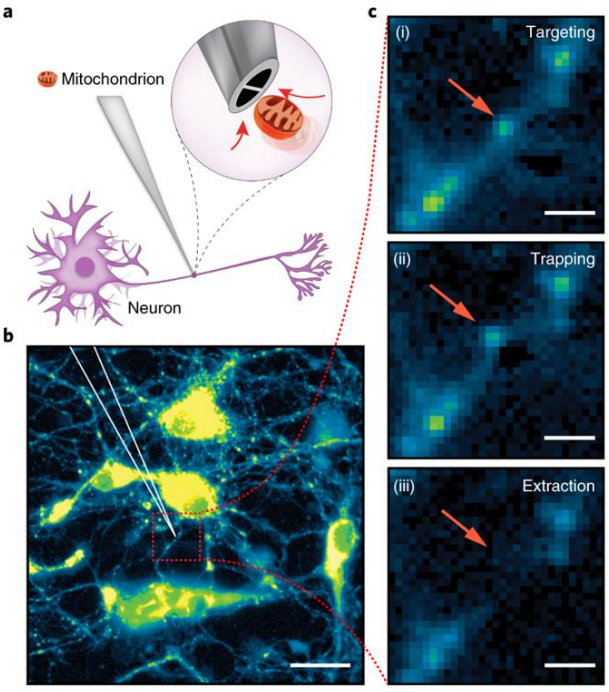

Figure 9 Single mitochondrion extraction with nanotweezers. a) Schematic of the extraction of a single mitochondrion from a neuron dendrite. b) Fluorescence micrographs after fluorescent staining of the mitochondria. c) Fluorescence micrographs showing (i) targeting of a single mitochondrion with the nanotweezers, (ii) trapping of the mitochondrion upon application of the AC voltage and (iii) extraction of the mitochondrion .

4.3 Fluid-force microscopy (FluidFM)

Another AFM- based approach for single-cell extraction is FluidFM, whereby a cantilever with a nanoscale tip containing a microchannel is attached to a pressure controller, allowing pressure driven liquid manipulation. Like DENT, FluidFM retains all the strengths of AFM, in that it can use force-feedback to precisely position the tip at the surface of the cell of interest, and precisely penetrate the cell membrane [136]. Guillame-Gentil et al used this technology to extract contents from living cells through the application of a negative pressure to the FluidFM tip, followed by downstream molecular analysis [137]. In this study, the pore at the end of the modified cantilever tip was 400nm in diameter, and the probe coated using surface silanization, in order to prevent the extracted contents from depositing on the microchannel and to facilitate the liquid flow.

First, extractions were performed from Green Fluorescent Protein (GFP)-expressing HeLa cells, and the authors demonstrated successful extraction by measuring the intracellular fluorescence decrease upon cytoplasmic aspiration. Next, the authors demonstrated spatially controlled extractions, sampling from the nucleus and the cytoplasm selectively in single cells. The nuclei of the single cells were labelled with the fluorescent protein mRuby, with a nuclear localisation sequence tag that causes it to be imported into the nucleus. Nuclear extractions using the FluidFM probe yielded a reduction in fluorescence intensity, whereas no decrease in fluorescence was observed upon extracting cytoplasmic contents, indicating mRuby had been extracted solely from the nucleus. Remarkably, when examining cellular viability post-extraction, the authors found they were able to extract up to 4.0 pL from the cytoplasm of HeLa cells with a cell survival rate of 82%. This represents a large proportion (around 90%) of the cytoplasm which is able to be extracted with minimal impact on cell viability. Additionally, when performing nuclear extractions, 86% of cells remained viable after extractions of up to 0.6 pL. To investigate the suitability of the FluidFM approach to be conjugated with mRNA analysis, the authors generated cDNA copies of transcripts from 2 housekeeping genes and GFP present in cellular extracts, followed by qPCR. They analysed the expression in different cytoplasmic extracts taken from GFP expressing cells, and confirmed the presence of transcripts for at least one of the genes in 90% of extracts, and all three in two thirds of extracts. Samples taken from the nucleus showed the presence of at least one of the genes in extracts ≥0.7 pL in volume. To build on this work even further, the authors later demonstrated the compatibility of the approach with metabolite analysis using matrix-assisted laser desorption ionization time-of-flight mass spectrometry (MALDI-TOF-MS). [138] In this paper, the authors identified 20 cytoplasmic metabolites extracted from HeLa cells using FluidFM followed by MALDI TOF mass spectrometry. Furthermore, by growing the cells on medium containing ^{13}C-glucose, they were able to demonstrate the incorporation of the heavier isotopes into cellular metabolites. In 2019, Aramesh et al used an adaption

of FluidFM to demonstrate intracellular detection of biomolecules and ions. [139]

Taken together these results show the ability to perform comprehensive structural and biochemical downstream analysis on subcellular extracts from cellular compartments using FluidFM with minimal impact on cell viability.

4.4 Nanopipettes

Another method to sample from living cells is based on the incorporation of nanopipettes within a Scanning Ion Conductance Microscope (SICM) [140]. SICM is based on an electrode-fitted nanopipette probe, immersed in a bath containing the sample of interest within an electrolyte solution. When a potential is applied between the working electrode inserted in the nanopipette and the reference electrode immersed in the bath, an ion current flows between the two. As the nanopipette reaches proximity to the surface of the sample, the ion current will drop as the ion flow will be hindered. Because the ion current is therefore distance dependent, it can be used as a feedback mechanism to control the distance between the tip and the sample, and as the pipette follows the sample surface, the movement of the pipette in the *z*-direction is measured to recreate the topography of the sample. SICM is a non-contact method used in solution, it is ideal for high-resolution imaging of live cells, and can recreate cellular topography in real-time [141]. Its force-free approach means that it can image delicate and intricate structures, such as neuronal networks and stereocilia [142], without the increased risk of sample damage or deformation experienced in techniques such as AFM, in which the sample encounters nonzero forces [143].

Nanopipette fabrication is simple and economical, employing a laser puller to pull a, typically quartz, capillary generating a nanopipette with a tip pore <100 nm in diameter [144]. Nanopipettes can be used to manipulate liquid using electrowetting. Here, the nanopipette is filled with an organic solvent and immersed into the aqueous bath, generating a liquid-liquid interface at its tip. A negative potential is applied between the nanopipette electrode and the bath electrode, altering the surface tension, and creating a force large enough to move the aqueous solution into the pipette. This volume correlates to the duration and magnitude of the potential applied, and it is possible to manipulate volumes as small as 1 attolitre using this technique [145]. One can therefore envisage a situation whereby the nanopipette filled with organic solution can be inserted into a living cell, harnessing electrowetting to extract the cytoplasmic contents.

Actis et al demonstrated the use of this technology, whereby they used nanopipettes to sample small volumes, on the femtoliter scale, from living cells [140]. The procedure is integrated with SICM, which enables the nanopipette to be precisely positioned above the cell membrane, following which the membrane is penetrated and cytoplasmic contents extracted by electrowetting. This process has minimal impact on cell viability, with a survival rate of >70%. The authors extracted contents from HeLa cells expressing GFP, and generated cDNA copies of the RNA extracted, confirming the extraction of GFP mRNA using real-time PCR. In addition to this, the compatibility of the nanobiopsy technique with next-generation sequencing was illustrated by sequencing the cDNA copies of the mRNA extracted from HeLa cells. This highlights the robustness of the approach for mRNA expression analysis from extractions from single living cells.

Furthermore, the authors were able to isolate mitochondria labelled with MitoTracker Green from live human fibroblast cells using the nanobiopsy set-up, and sequenced the mitochondrial genomes using next-generation sequencing. In 2018, Toth et al employed the nanobiopsy platform to investigate mRNA compartmentalisation in neurons [146]. The authors aspirated cytoplasmic extracts from different locations within the same cell, both in the cell body and the neurites, and employed next-generation sequencing to analyse the extracts. The authors found 1292 genes expressed in the cell body, and 929 in the neuronal body. It was clear that the neurites and cell body had different mRNA expression profiles, with an overlap of only around 200 genes, which is has functional significance. In addition, some species of mRNA which were functionally related localised to the same area within the cell. Not only this, 178 mRNA transcripts were detected in neurite nanobiopsies which were low in abundance and have not been detected in bulk analysis in the past, demonstrating the sensitivity of the technique. Among these mRNA species were transcripts which were previously believed to be contained only in the nucleus, and were here detected in neurites for the first time. Overall, the authors demonstrated localisation of mRNA within neurons as well as proving the ability of the nanobiopsy platform to be used multiple times within the same cell and its sensitivity and its compatibility with next-generation RNA sequencing.

These studies have only taken advantage of SICM- controlled positioning of nanopipettes in the z-axis. To build upon this, Nashimoto et al. integrated two fundamental capabilities of nanopipettes; i.e. the ability to aspirate cellular contents via electrowetting, and the ability to generate a complete topographical image of a cell via SICM [147]. As the ion current magnitude from a nanopipette filled with organic solution (dichloroethane) is too small for accurate mapping in the x-y axes, the authors used a dual-barrel nanopipette with an aqueous-phase barrel serving as an SICM probe to generate a topographical map of the cell and an organic phase barrel to aspirate cytoplasmic contents. The topographical images of individual mouse fibroblast cells created using the aqueous barrel were used to precisely position the pipette, in order to sample from different regions within the same cell, and analysis of the extracts provided information on mRNA localisation within the cells. The same group in 2019 demonstrated

that electrowetting-driven cell aspiration can also be performed within tumour spheroids to study differential gene expression at the surface and at the interior of the spheroid [148].

Nanopipettes can also be used under pressure control to aspirate samples from living single cells. Saha-Shah et al extracted cytosolic fractions of around 8 nL from *Allium cepa* single cells with a nanopipette 600 nm in diameter, followed by analysis by matrix assisted laser desorption ionisation mass spectrometry (MALDI-MS) and identified hexose-oligosaccharides. Furthermore, the technique was extended to lipid analysis mouse brain tissue slices and first instar *Drosophila melanogaster* larvae. Altogether this demonstrates the versatility of the approach for use in plant cells, tissue samples and complex biological samples, as well as the compatibility with mass spectrometry identification of both hydrophobic and hydrophilic molecules.

These results collectively show the wide-reaching capabilities of nanopipettes in use for single-cell analysis studies, being able to extract content from varying cell types, their compatibility with next-generation sequencing and mass spectrometry, and the ability to isolate and analyse individual organelles[149, 150]. Additionally, the conjugation with SICM allows precise positioning of the probe, and multiple extractions from the same cell in defined locations.

4.5 Nanostraws

A different method of performing extractions from living cells is using 'nanostraws' [151-153]. Here, cells are cultured in a dish with a membrane at the base, containing hollow cylindrical tubes, 150 nm in diameter, which project upwards. A voltage is applied through the nanostraws, which electroporates the cells, giving the nanostraws cytoplasmic access through the temporary holes created in the membrane near the nanostraw tip, for 2-5 minutes (Figure 10). This allows intracellular contents to travel through the nanostraws, by diffusion, into a reservoir containing buffer solution below, which can then be collected and analysed. As such, the extracts from each cell are collected in the same bath and analysed together. The sampling area can be defined using photolithography, enabling sampling from regions <1μm to mms in size.

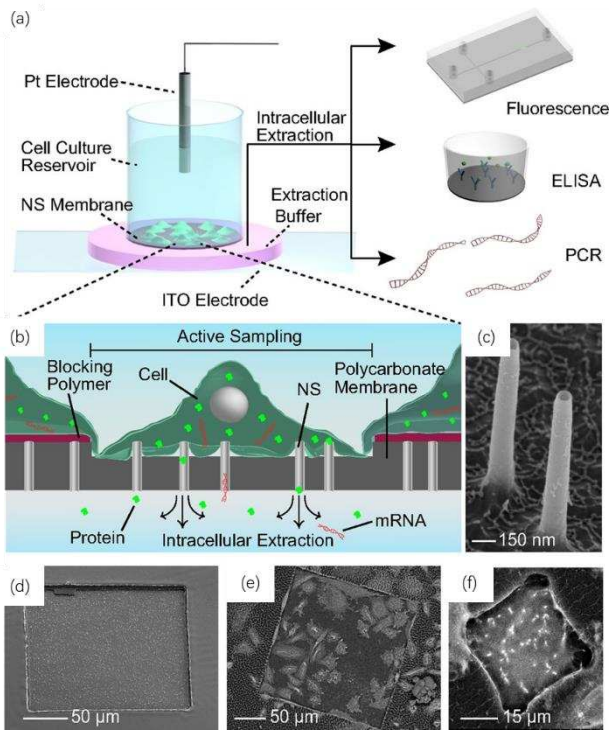

Figure 10 Schematic of the nanostraws technology. (a,b) This sampling technique is based on a polycarbonate membrane with protruding 150-nm diameter nanostraws supported on a cell-culture dish. Sampling is triggered by the application of short voltage pulses that temporarily electroporate the cells, allowing cellular content to diffuse through the NS and into the underlying fluidic reservoir (highlighted in pink in a)), which is then analysed using fluorescence imaging, ELISA, or qPCR. (c,d) SEM images of the 150 nm diameter NS (c) and the 200 × 200 μm2 active sampling region (d). Cells outside this window are unaffected by the sampling process. (e,f) SEM images of cells cultured on a 200 × 200 μm2 active sampling region containing 42 cells (e) and a 30 × 30 μm2 sampling region used to isolate and sample from a single cell (f).

To illustrate the efficacy of this approach, Cao et al. periodically sampled from an area of 38 GFP and Red Fluorescent Protein (RFP)-expressing CHO cells and verified successful extraction by measuring the fluorescence intensity of the extracts using fluorescence microscopy. The sampling area was then decreased in order to sample from a single cell, and the amount of RFP extracted over a 4-day period was measured pre- and post-transfection with an RFP plasmid at day 2. The authors found that the increase in the RFP content of the extracts correlated with the increase in RFP expression by the cell. The resulting cell viability was >95%, showing the ability of this technique to sample from cells longitudinally and non-destructively.

The authors further validated the nanostraw platform as a longitudinal live cell-sampling method by sampling from human induced pluripotent stem cell (hiSPC)-derived cardiomyocytes and astrocytes over a 5-day period. They used an enzyme-linked immunosorbent assay (ELISA) to detect the heat shock protein 27 (HSP27) in extracts following the incubation of cells at 44°C for 30 minutes. An upregulation of

HSP27 expression was observed after the heat shock. This was performed on an area containing 100 000 cells, in order to be compatible with the ELISA sensitivity. Finally, mRNA was extracted from hiSPC-derived cardiomyocytes, and the expression of a selected set of mRNAs was analysed, compared to a lysed cell. All mRNAs detected in the lysed cell were also present in the nanostraw-derived extract. This process required 15-20 cells for sufficient mRNA analysis, however, there is the possibility for single-cell mRNA expression detection to be performed in the future as mRNA analysis techniques become more sensitive. Furthermore, contrary to other techniques outlined in this review, nanostraws allows parallel extraction from cells, rather than consecutive sampling.

4.6 Nanotube endoscopes

Singhal et al have demonstrated that a carbon nanotube that be inserted within the tip of a micropipette to comprise a nanoscale endoscope able to penetrate a cell membrane to perform intracellular analysis[154]. The authors demonstrate that the carbon nanotube can be decorated with gold nanoparticles and Surface Enhanced Raman Spectroscopy (SERS) spectra can be acquired within the intracellular space. The authors also hint at the potential for single-cell surgery by showing some preliminary data on single organelle probing but do not perform any downstream molecular biology analysis. Similarly, Yan et al [155] attached a nanowire on the tip of a tapered optical fibre to comprise a nanowire endoscope. The authors employed it for intracellular cargo delivery and for optical interrogation of intracellular compartments with nanoscale resolution. Although both these nanoendoscope techniques have not been used for extraction of cellular contents they both hold great promise for simultaneous detection and extraction of intracellular material.

5. In vivo electrochemistry in brain research: challenges and solutions

To explore the molecular mechanism and chemical information of brain function is one of the important frontiers of modern neuroscience, and brings both great challenge and opportunity to chemists. While we are still in the learning phase in many aspects of brain chemistry, the electroanalytical community is certainly making significant advances down this path, with a broad range of micro-sized and chemically engineered electrodes that have proven to be highly effective in measuring rapid chemical changes in live animal brains.

5.1 Overcoming the in vivo selectivity challenge by modulating the interfacial electron transfer

There are many types of chemical substances exist in the brain, which are unevenly distributed, and transformed in an exquisitely ordered manner. It therefore remains as one of the most challenging issue to selectively measure the neurochemical in such a complicated environment, particularly in a live brain. The traditional approaches for sensitive in vivo electrochemical analysis rely on the development of new electrochemical technologies that discriminate neurochemicals based on their own voltage-dependent oxidation and reduction processes. For instance, fast scan cyclic voltammetry (FSCV) as a typical technology has garnered considerable interest in neurochemical research community. At the ultrafast scanning speed, neurochemicals of different electron transfer kinetics can become distinguished as their redox peaks shift to distinct positions. By virtue of its selectivity and millisecond temporal resolution, over the past 20 years, FSCV has been extensively adopted to study the dynamics of neurochemicals, such as dopamine and serotonin in live animals. However, being a background-subtracted method, FSCV inherently requires complicated data collection, analysis and statistic models to improve the signal resolution. Moreover, great efforts have also been contributed to extend its suitability to neurochemicals that are less electroactive,[14] which greatly restrict FSCV from the wider in vivo analysis applications.

We began to work on selective in vivo analysis strategy and principles since 2002, and focus on designing new chemical approaches to modify electrode surface, and to modulate the electron transfer at its interface, enabling in vivo electrochemical monitoring of brain chemistry with excellent selectivity. The very first example in this line was demonstrated by using carbon nanotubes (CNTs) to construct electrode/electrolyte interface for selective electro-oxidation and in vivo analysis of Vitamin C (VC, also named as ascorbic acid, AA). We found that VC oxidation can be greatly accelerated on heat-treated CNTs, primarily owing to the presence of edge plane-like carbon and excellent electronic properties of CNTs.[156] More importantly, the CNTs-facilitated electron transfer works nicely when it was integrated with in vivo analytical system, allowing selective determination of VC against interfering neurochemical species in the central nervous system (CNS).

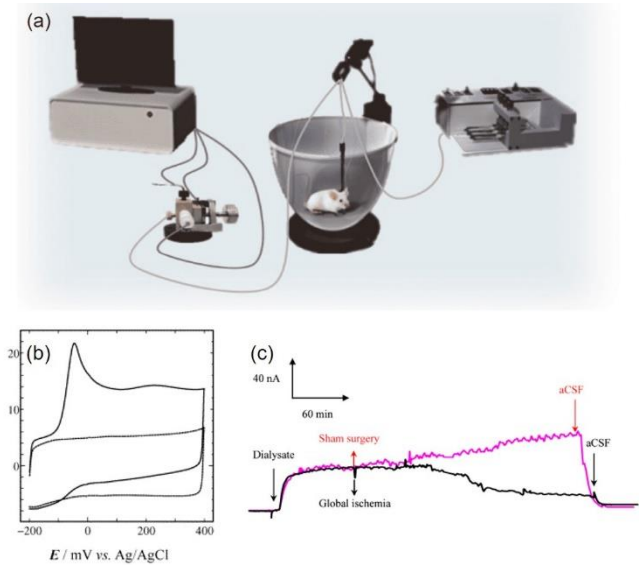

Figure 11 (a) Schematic diagram of analytical system for selective determination of VC in rat brain. Reprinted (adapted) with permission from ref. [157] Copyright (2019). (b) Typical cyclic voltammograms (CVs) obtained at heat-treated CNTs modified-electrodes in the presence (solid lines) and the absence (dash lines) of VC. (c) Online measurement of VC in the brains of ischemia rats (black line) and shame-operated rats (red line). Reprinted (adapted) with permission from ref [158] Copyright (2005).

Venton et al. reported the use of CNTs modified carbon fiber microelectrodes for monitoring simultaneous release of dopamine and serotonin in vivo. To further improve the electrocatalytic performance of CNTs, Zhang et al. engineered tunable defects and oxygen-containing groups in CNTs which exhibited a greatly facilitated VC oxidation at a low potential, allowing in vivo detection of VC levels in rat brains under both physiological and pathological conditions. Besides CNTs, carbon black also serves as an excellent electrode material owing to its merits of high conductivity, large surface area and low cost. For example, by coating nano-composites of carbon black and mediator onto electrode surface, Cheng et al. constructed a ratiometric electrochemical sensor for selective VC measurement in live brains [158].

The successful modulation of electron transfers by tuning the surface chemistry of electrode using CNTs further inspired our studies of other carbon nanomaterials that feature distinct chemical and physico-chemical properties, such as graphdiyne. We found that oxidized graphdiyne (GDO), which contains a large degree of electron-withdrawing acetylenic bonds, exhibiting an ultrafast humidity response with an unprecedented response speed (ca. 7 ms). Such chemical attributes along with its electrochemical properties enable us to fabricate a GDO-based humidity sensor with excellent selectivity against other types of gas molecules, and allow accurately monitoring of the respiration rate change in living systems. Inspired by the electrochemical attributes of carbon nanomaterials, we reason that the single-atom catalyst (SAC), featuring atomic active sites that are dispersed in ordered porous N-doping carbon matrix, could be superior in catalyzing the electrochemical process of physiologically relevant chemicals. As demonstrated very recently by our group, we found that a cobalt-based single-atom catalyst (Co-SAC) can catalyze the electrochemical oxidation of hydrogen peroxide (H_2O_2) at a low potential of ca. +0.05 V(vs. Ag/AgCl), therefore, allowing for the further development of an oxidase-based biosensor for selective monitoring of glucose in rat brain.

Other than using synthetic nanomaterials to tune the interfacial chemistry of electrode for selective in vivo analysis, enzyme-modified electrodes remain particularly attractive in developing sensors with high selectivity. Generally, flavin adenine dinucleotide (FAD)-containing oxidases and dehydrogenases are two types of enzymes that have been widely employed to construct electrochemical biosensors, in which the oxidase-based biosensors are more popular for in vivo analysis. This is because their ease in fabrication with less interference from hydrogen peroxide, one of the most abundant, small-molecule oxidants exist in the cerebral systems. Nevertheless, the requirement of using mediators, for example ferricyanide/ ferrocyanide ($Fe(CN)_6^{3-/4-)}$ whose redox potential generally overlaps with those endogenously existing neurochemicals in the cerebral systems makes them far from ideal for in vivo neurochemical measurements. To realize the negative shift of the redox potential of $Fe(CN)_6^{3-/4-}$, we have developed the modification of an imidazolium-based polymer (Pim) onto electrode, controlling the different adsorption ability of $Fe(CN)_6^{3-}$ and $Fe(CN)_6^{4-}$ onto electrode surface [159]. This strategy has led to a negative shift of the redox potential of the surface-confined redox mediator. Using glucose oxidase (GOD) as the model recognition units, we have demonstrated the validity of the ferricyanide-based second-generation biosensors for selective in vivo glucose measurements.

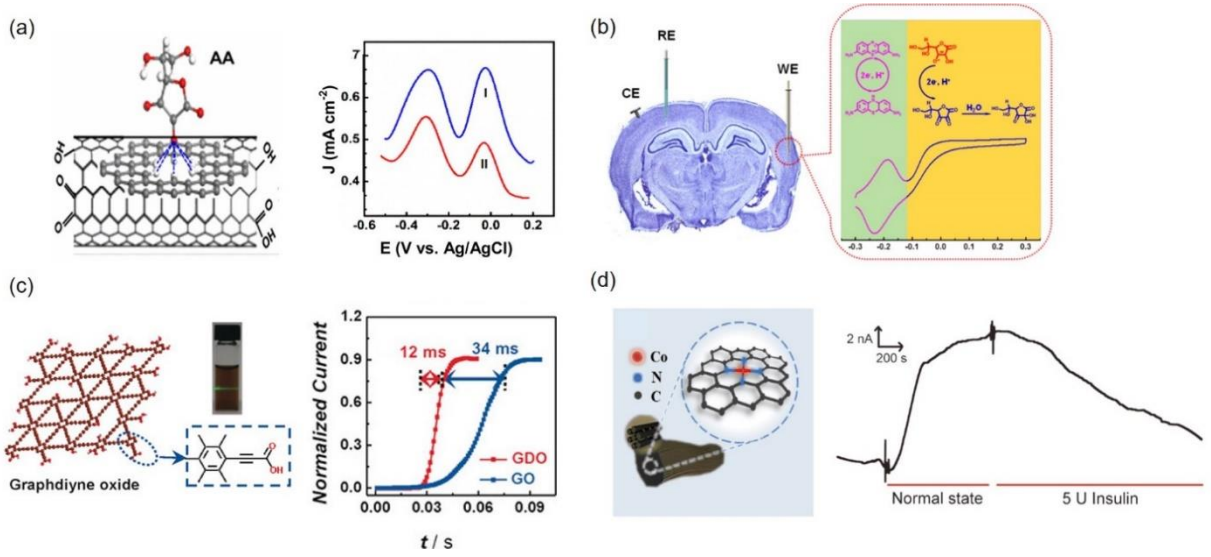

Figure 12 (a) The absorption of AA on defect-containing CNTs and differential pulse voltammetry (DPV) records obtained in the striatum of normal rat (blue line) and rat model of Alzheimer's Disease (red line). Reprinted (adapted) with permission from ref. [160] Copyright (2017); (b) Schematic illustration of ratiometric electrochemical sensor for measuring AA in live brains. Reprinted (adapted) with permission from ref.[158] Copyright (2015); (c) Schematic illustration of Graphdiyne oxide (GDO) and current responds of both GDO-based (red line) and Graphene oxide (GO)-based (blue line) sensor toward humid air. Reprinted (adapted) with permission from ref.[161] Copyright (2017); (d) Schematic illustration of Co-SAC and typical amperometric responses from rat striatum under normal state and after injection of insulin. Reprinted (adapted) with permission from ref. [157] Copyright (2019)

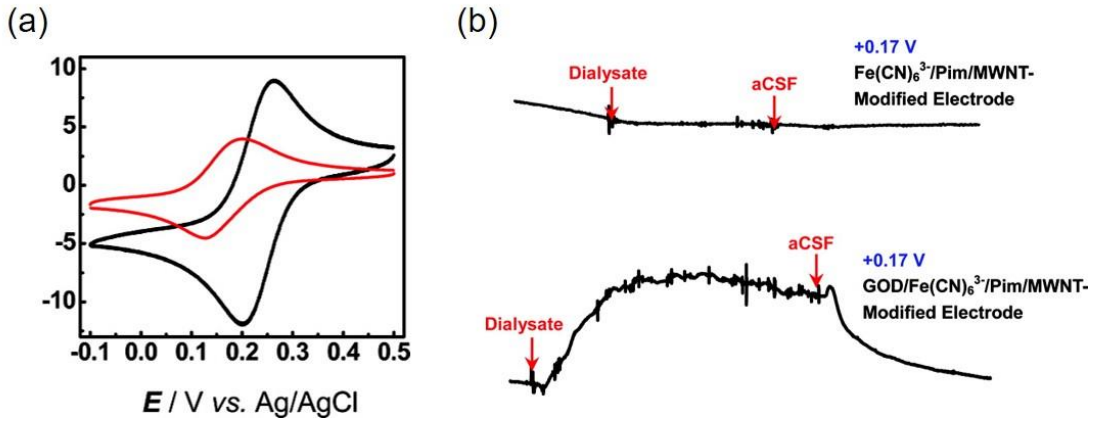

Figure 13(a) Typical CVs obtained at multiwalled CNTs (MWNTs) modified electrode (black line) and Fe(CN)63-/Pim/MWNT-modified electrode (red line). (b) Typical amperometric response of microdialysate sampled continuously from the striatum of guinea pigs. Reprinted from [159] with permissions. Copyright (2012).

Given the great variation of pH and oxygen levels involved in most of the physiological and pathological processes, a sensor with high tolerance against oxygen and pH would be the most desirable for in vivo measurement. Since the dehydrogenase-based catalytic chemical oxidation of glucose and lactate is oxygen-independent, we adopted the dehydrogenase as the recognition element on the electrode surface and developed dehydrogenases based electrochemical system that allows selectivity monitoring of glucose and lactate in brain with minimal interference from pH and oxygen [162].

Taken together, the use of synthetic nanomaterials or naturally existing enzymes as electrocatalysts to modulate the interfacial electron transfer of electrodes have proven to be efficient and contributed significantly in solving the long-lasting challenge in the selective in vivo analysis of neurochemicals.

5.2 Overcoming the in vivo stability challenge by developing the Galvanic Redox Potentiometric (GRP) sensors

Amperometry permits selective and sub-second in vivo measurements of neurochemicals, allowing their wide use to elucidate the physiopathological roles of neurochemicals in animals. However, one of the main drawbacks associate with amperometry is the instability of electrode in vivo, which re-

sults in a dramatic drop in current due to the electrode passivation by nonspecific adsorption of proteins in biological fluids. These issues affect the relationship between the current and the concentration restricting a stable in vivo measurement. In this regard, determining the basal levels and monitoring the dynamics of neurochemicals require the in vivo analysis to be sensitive yet stable in the complex environment. In view of this challenge, potentiometric measurements based on Nernst equation is gaining in prominence because they are less affected by the surface area of working electrodes. One of the best-known potentiometric sensors is ion-selective electrode (ISE), which is widely utilized to determine ion concentration by measuring transmembrane potential. Being implanted in rat brains, ISEs has extended the applications for in vivo measurement of K^+, H^+ and Ca^{2+} [163, 164]. Recently, a fluorescent nanosensor has also been used for in vivo monitoring of extracellular K^+ levels in the brain [165].

In addition to ions, we have designed the very first open-circuit potentiometric-based sensor, termed galvanic redox potentiometric (GRP) sensor, for measuring the molecular dynamics of neurochemicals in live brain with satisfying selectivity, unaltered sensitivity by electrode fouling, and high reliability.[165] The direct electron transfer (DET) of laccase on CNT-modified electrodes allows the construction of Galvanic cell, through which the oxygen can be reduced at a high potential where the thermodynamics allowed, providing the foundation for the establishment of GRP method. Moreover, we observed a dramatic enhancement of oxygen reduction current response (by ca. 600% at maximum) upon ethanol-assisted immobilization at carbon nanotube electrodes, achieving both high potential and high current simultaneously, which provides the possibility of using laccase electrode as reference electrode of GRP. The GRP sensor overcomes many scientific bottlenecks, such as the realization of the direct electron transfer of laccase and construction of Galvanic cell, successfully transforming the detection of redox active substances from traditional current-based method to potential-based approach, providing new electrochemical principles to solve inherent stability issues in current in vivo analysis systems.

While the GRP sensor has been demonstrated to be very attractive for stable in vivo analysis, the selectivity remains a big concern. The use of enzyme-based biosensing strategy would pave an effective way to this problem. Very recently, we have used recombinant Ferredoxin-dependent glutamate synthase (Fd-GltS) from cyanobacteria as an enzymatic bioelectrocatalyst to develop a new electrochemical biosensor for glutamate detection. Particularly, bioelectrocatalytic oxidation of glutamate by Fd-GltS was oxygen-independent, overcoming the challenges that associated with oxidases or dehydrogenase-based bioelectronic sensors, which are oxygen dependent, and the requirement of co-enzymes, respectively. Moreover, as the redox centers of Fd-GltS are close to enzyme surface, making it prone to realize direct electron transfer with the electrode. Taken together, it is favorable to use GRP principles to develop new-generation of electrochemical sensors for in vivo analysis of glutamate.

With all above efforts, we further extended the GRP strategy for in vivo monitoring of VC, as a proof-of-concept study. The GRP sensor is constructed on a self-driven galvanic cell, where VC is spontaneously oxidized at the indicating single-walled carbon nanotube modified electrode (SWNT-CFE), while oxygen reduced at the laccase-modified reference CFE (Lac-CFE). The as-designed sensor shows a high selectivity to VC in the presence of coexisting electroactive neurochemicals. It further enables the measurement of the basal level of cortical VC in live rat brain (230 ± 40 μM) and its fluctuation during ischemia/reperfusion. It is worth of note that the sensitivity of GRP sensor is tolerant to protein adsorption or electrode fouling, offering a prominent method for in vivo, real-time, stable and reliable analysis of brain neurochemistry.

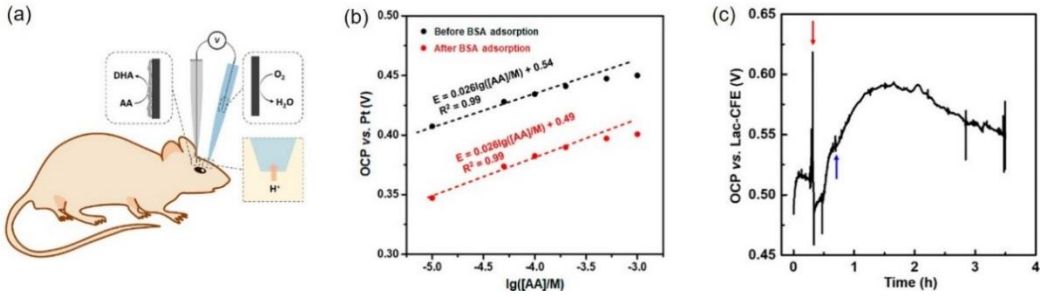

Figure 14 (a) Schematic illustration of in vivo AA monitoring by using GRP sensor. (b) Calibration curves of the GRP sensor before (black line) and after (red line) BSA adsorption. (c) In vivo AA monitoring during global cerebral ischemia (red arrow) and reperfusion (blue arrow). Reprinted (adapted) with permission from ref. [165] Copyright (2018)

5.3 Neurobiology studies enabled by new in vivo analytical methods

Monitoring the dynamic change of neurochemicals in living animals can provide important information for understanding the molecular mechanism of CNS, as well as the cause of neurodegenerative disorders. The key challenges associated with brain chemistry research lie in the deciphering of neurochemical signaling in terms of its chemical, spatial, and temporal information. In this regard, in vivo electrochemical monitoring of neurochemical is of great potency for above-mentioned neurobiological studies. For example, our in vivo electrochemical systems, established either through modulating the electron transfer by engineering of interfacial chemistry or outputting signals using potential-based GRP method, have been demonstrated to be satisfyingly selective and stable in monitoring of neurochemical fluctuation in living brain of animals with high temporal and spatial resolution. Specifically, being able to deploy micro-sized sensors into specific region of brain, has been the cornerstone for the realization of in situ monitoring of a great variety of neurochemicals, including VC [166], dopamine [167], glutamic acid [168], oxygen [169], glucose [170], lactic acid [171], hypoxanthine [172], ATP [173], and H_2S [174], offering new analytical approaches for advancing our understanding of the brain science.

Particular exciting is that with our *in vivo* analysis system, we demonstrated that VC might exhibit some unexplored roles in certain physiological events associated with brain diseases. For example, we found that VC can be released in the form of nanoscale vesicles, the main pathway that is commonly preserved in the regulated secretion of neurotransmitters by neurons (Figure 15(b)).[175] Moreover, we observed for the first time that the propagative nature of VC release following the spreading diffusion process, highlighting its importance as a neuromodulator in mediating neurotransmission (Figure 15(a)).[176] Furthermore, through our long-term collaboration with Peking University Third Hospital, which specializes in designing, establishing and evaluation of clinical relevant disease models, we demonstrated that VC plays more important roles other than just as free radical scavengers for neuro-protection in the events of tinnitus , olfactory dysfunction and Vertigo [177].

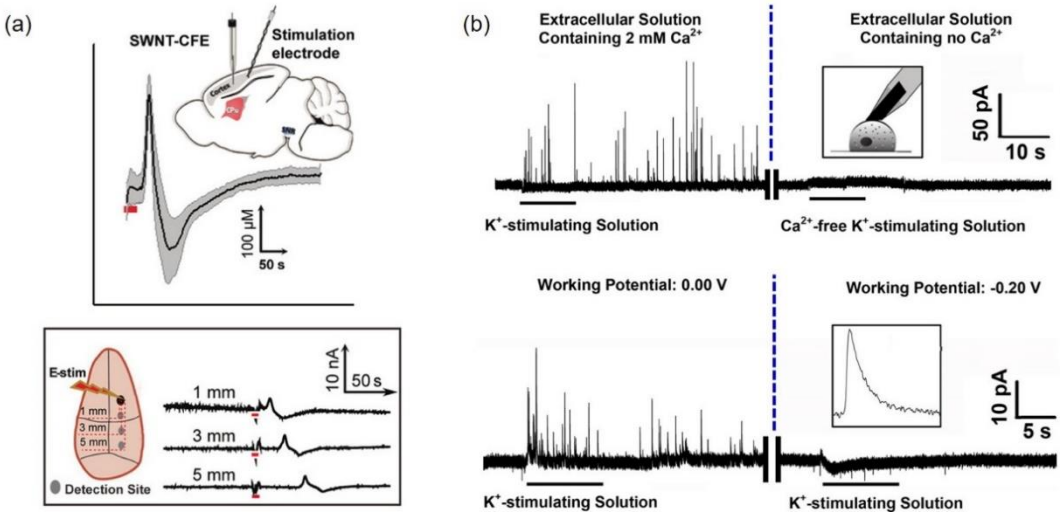

Figure 15 (a) Typical current recordings upon electrical stimulations (red bars), insert, schematic illustration of experiment setup (top) and VC release in different detection sites followed by electrical stimulations (red bars) (down). Reprinted (adapted) with permission from ref. [176] Copyright (2019); (b) Single-cell amperometric recordings of vesicular VC release by K+-stimulated exocytosis. Reprinted (adapted) with permission from ref. [175] Copyright (2017)

Most importantly, the approach for in vivo analysis of glucose, lactic acid, ATP, glutamic acid, pH, calcium ions and other neurochemicals, has been demonstrated to be profoundly effective by some domestic institutes and hospitals in their own independent research. This interest in using the in vivo electrochemical sensors can be attributed to their excellent selectivity and stability, two essential prerequisites for reliably capturing and further interpreting the dynamics of neurochemicals in the complicated central nervous system. The application of our in vivo electrochemistry based neurochemical sensors has provided a solid experimental foundation for exploring molecular mechanisms of brain function and highlighting the key role and bright future of analytical sciences in brain research.

6. Towards precision electrochemical measurements

The challenge in developing meaningful and fundamentally accurate descriptions of complex electrochemical mechanisms, e.g., the multi-step reduction of O_2, is in understanding the interfacial structure with a high degree of precision, and by improving the temporal and spatial resolution of methods to interrogate reactions.

Over the past decades, electrode fabrication in the micro- and nano-domains has allowed studies of single entities ranging from individual molecules to single nanobubbles, pushing

analytical electrochemistry to the regime of unit sensitivity with unprecedented precision at the single-entity scale.[1, 178, 179] Nanoelectrodes offer significant advantages over macro and microelectrode geometries in probing chemical and kinetic properties at the individual molecule or nanoparticle scale. Often this is done by coupling extremely small background double-layer capacitance values with near-instantaneous steady-state concentration profiles to offer the spatiotemporal resolution necessary to probe electron transfer kinetics in the nanosecond regime [180-182]. In recent years, the employment of nanoelectrodes in electrochemical microscopy techniques has become increasingly important to study a wide variety of different reactions [183-185], and to elucidate the localized structure-activity in a wide range of electrochemically active nanomaterials (e.g., nanotubes, graphite and graphene, nanoparticles, and materials for energy storage) [185, 186]. These precision measurements pave a new way to explore mechanisms of complex chemical process, expanding analytical applications for electrochemistry.

6.1 Counting molecules in nanobubbles

Gas generation with phase formation is important in both fundamental studies of nucleation and many electrocatalytic processes.[187, 188] Nucleation, the first step of phase formation, takes place in a very short time at nanometer length scales. While classical nucleation theory (CNT) describes average rates of nucleation,[189] direct and precise measurements of the nucleation of single gas nuclei are barely reported.[190-192] Therefore, a detailed quantitative measurement of the behavior of nanobubbles on the electrode surface is of great importance.

A single-entity approach was recently developed to analyze the nucleation of single nanobubbles from precise measurements at nanoelectrodes.[193] Taking H_2 bubble formation as an example (Figure 16(a)): during the voltammetric scan, when hydrogen evolution reaction occurs, the concentration of dissolved H_2 near the electrode surface increases as the current increases. When the concentration of H_2 is sufficiently high, a H_2 bubble nucleates stochastically from the supersaturated solution, and rapidly grows and covers the electrode surface. This coverage blocks the active electrode surface, causing a sudden decrease of the current, resulting in a peak current, $i^{p}_{H_2\ nb}$, in the voltammogram. The peak current occurs at the moment when H_2 bubble nucleates and can be used to calculate the concentration of H_2 required for nucleation.

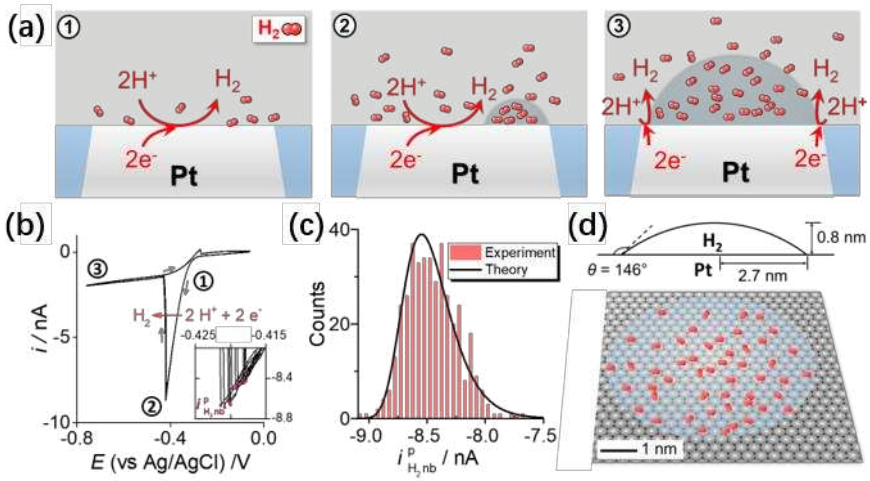

Figure 16. (a) Schematic of the nucleation and growth of a single H_2 nanobubble on a Pt nanoelectrode: 1. H_2 produced by proton reduction remains dissolved. 2. A critically-sized nucleus forms. 3. A single stable bubble covers nearly the entire electrode. (b) Cyclic voltammogram showing bubble formation at a 10 nm Pt disk electrode in 1.0 M H_2SO_4 (10 cycles shown); numbers relate to stages in part a. (c) histogram of nucleation peak currents ($i^{p}_{H_2\ nb}$) from 400 voltammetric cycles and theoretical fit using $J_0 = 6.3 \times 10^{12}$ s^{-1} and $\theta = 150°$. (d) Schematic of the critical nucleus for H_2 bubble derived from analysis of $i^{p}_{H_2\ nb}$ in the voltammograms in b). Reproduced, with modification, from ref. [193] copyright 2019 by the American Chemical Society.

Further information of bubble nucleation rate and properties of the critical nucleus can be obtained by analyzing the distribution of $i^{p}_{H_2\ nb}$. The experimentally obtained $i^{p}_{H_2\ nb}$ in multiple voltammetric cycles is highly reproducible (~3% relative deviation, see Figure 16(b) and (c)), even though nucleation of a single bubble is stochastic, as has been demonstrated in previous induction time measurements for single bubble nucleation.[194] This seemingly deterministic behavior of $i^{p}_{H_2\ nb}$ can be explained by applying classical nucleation theory and statistics (survival analysis) to the voltammetric response. The experimental distribution of $i^{p}_{H_2\ nb}$ in hundreds of voltammetric cycles can be well fitted by the theory (Figure 16(c)) using two free variables in classical nucleation theory; the pre-exponential factor J_0, and the contact

angle of the bubble nucleus, θ.

With the theoretical analysis, a voltammetric approach was developed to measure parameters of the nanoscopic bubble nuclei by analyzing the small variation, i.e., the "noise", in the peak current. The distribution of the peak current for nucleation is precisely measured in multiple voltammetric cycles and the distribution of this value is fit by theory using combination of J_0 and θ. It is found that a H_2 bubble nucleus has a contact angle of 150° (Figure 16(d)). Together with the pressure inside the bubble nuclei, also calculated using the voltammogram, the number of H_2 molecules in a H_2 bubble nucleus is ~ 50. This voltammetric approach can also be applied to the nucleation of bubble of other gas types, including N_2, O_2, and CO_2. Such an approach demonstrates the power of single entity electrochemistry.

6.2 Sub-nanometer resolved particle size measurements

Achieving precise information about single entities, requires one to minimize the influence of extraneous sources of noise. While careful choice/design of electronic circuitry, appropriate grounding, and shielding from electromagnetic radiation (e.g., through using a Faraday cage), are an advisable first course of action, in order to minimize the influence of electrical noise, further improvements require additional strategies. Repeated measurements of the same quantity are commonly performed in analytical chemistry, as a means to improve measurement precision. While repeated measurements of individual nanoscale entities may present new measurement challenges, in addition to improved precision, they can provide additional information, e.g., through characterizing the distribution of an inherently stochastic quantity, or by observing processes that would be averaged over in an ensemble measurement.

As described in Section 2, in resistive pulse sensing, the ion current between two electrodes, one inside an electrolyte-filled nanopipette/nanopore, the other in bulk solution (Figure 17(a)), is used to characterize a single nanoscale entity as it passes through the pipette/pore orifice. The momentary drop in current that occurs as an entity translocates provides information on its size, shape and more [28]. Using computer-controlled instrumentation, which facilitates repeated resistive pulse measurements of individual nanoparticles in solution, an augmented resistive pulse sensing method was developed, which allows measurements of individual particle properties with enhanced precision,[195] and facilitates new measurements. [196]

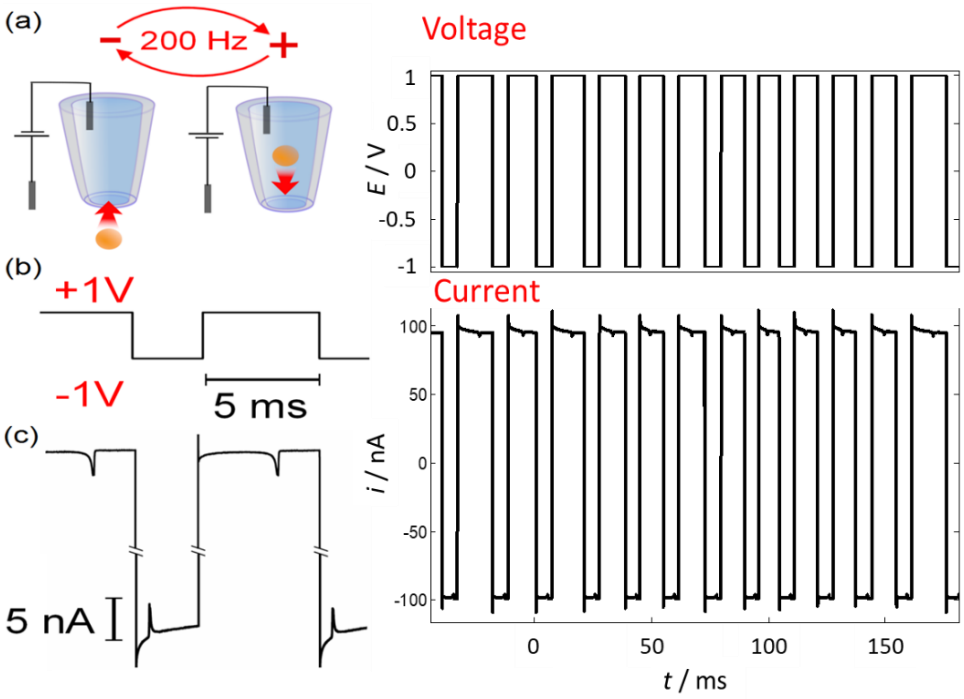

Figure 17. Multipass resistive pulse sensing of a single nanoparticle. Adapted from ref. [197], copyright American Chemical Society.

As shown schematically in Figure 17(a), a nanoparticle passing through the orifice of the nanopipette, is detected by a resistive pulse and, after a predetermined (~ms) delay, the direction of the forces acting upon the nanoparticle are automatically reversed.[198] In the example shown, reversing the polarity of the applied potential (Fig 17(b)) reverses the net force on the particle. In this case, the forces arise from elec-

troosmotic flow and electrophoresis, but altering the hydrostatic pressure across the pore can achieve a similar result. [195] The reversed forces drive the particle back through the orifice, whereby another resistive pulse is detected, and the wait-switch-detect cycle repeated. Figure 17(b)/(c) shows the potential/current-time traces corresponding to four resistive pulses from the same particle passing out-in-out-in, which were taken from the larger dataset shown on the right hand portion.

The exclusion of conductive electrolyte, equal in volume to the particle typically causes the largest contribution to the amplitude of the resistive pulse; however, variability in the amplitude arises from variability in the position of the particle as it translocates, relative to the pore axis.[199] Repeated measurements of the same particle can eliminate (and characterize) this variation, thus with sufficient measurements of the same particle (>10,000 demonstrated [197]) the volume of a single particle can be characterized with essentially arbitrary precision.[195, 197]

When non-spherical objects translocate, the resistive pulse reflects both the orientation and volume of the object. For example, a nanorod with its long axis parallel to the axis of the pore gives a lower resistive pulse amplitude compared to that of a sphere of equal volume, whereas when the axes are perpendicular, this relationship is reversed. Moreover, if the orientation of a particle charges during translocation local maxima and minima are observed in the otherwise smooth resistive pulse. Analysis of the time between peaks informs on the tumbling rate, which we related to the rod shape through equations of rotational diffusion.[200]

While the amplitude of the resistive pulse is typically dominated by the volume of entity that is translocated, the shape of the resistive pulse contains additional information, including on the surface charge,[201] bipolar electrochemistry ,[202] and the mechanical properties of soft entities.[203]

The combination of nanoparticles and nanopipettes extends beyond resistive pulse sensing.[204] When a pipette is placed close to an electrode resistive pulse characterization can be combined with delivery of a particle to a surface, allowing for correlated electrochemical characterization and probing of the dynamics of particles.[205-207] While such tandem measurements have not been combined with the extra precision of multipass measurements, it seems only a matter of time before they are.

6.3 Towards electrodes of molecular dimensions

Precision measurements based on nanoelectrodes have been integral in revealing physicochemical properties at single molecules and nanoparticles; however, reproducible and representative measurements at this length scale necessitate robust nanoelectrode fabrication techniques to extract meaningful insight. Since 2001, with the seminal work of Katemann and Schuhmann describing platinum disk nanoelectrodes fabricated *via* laser pulling of quartz-sealed Pt microwires and subsequent focused ion beam (FIB) milling to expose the Pt surface,[208] robust bench-top techniques to generate a wide range of nanoelectrode geometries have been described including inlaid disks,[182] nanopore,[181] nanogap,[209] nanoelectrode arrays,[210] and nanoparticle electrodes.[211] These techniques have been extended beyond Pt, to generate Au,[212] Ag,[91] Cu,[213] and C nanoelectrodes [214, 215] offering a wide range of electrode materials suitable for fundamental electrochemical studies of both inner- and outer-sphere electron transfer processes. While these nanoelectrodes offer unparalleled electrochemical sensitivity at the single entity level, the stability of nanoelectrodes following fabrication and during repeated measurements remains a challenge in precise single entity studies. [1] As highlighted in Amemiya's 2013 work on electrostatic discharge damage to Pt nanoelectrode surfaces, extensive care must be taken to ensure the geometry of a nanoelectrode has not been perturbed prior to or during an electrochemical measurement.[216] While electrode fouling *via* organic molecule adsorption can be countered with plasma treatment [217] or FIB milling to re-expose the nanoelectrode, operator handling of these electrodes during the cleaning process introduces another opportunity for electrode fouling. FIB milling of laser-pulled quartz-sealed Pt wire nanoelectrodes remains the preferred method for fabricating low RG nanoelectrodes (RG is R_g/a, where R_g is the radius of the insulating glass and a is the radius of the microwire) for nano-SECM or in-vivo single cell measurements. However, high RG nanoelectrodes can be generated by sealing either a) cyanide etched Pt or Au wires or b) pulled quartz-sealed Pt nanoelectrodes in a larger capillary and mechanically polishing the electrode on an alumina polishing pad with an electrical continuity probe to indicate nanoelectrode surface exposure .[182] Pt nanoelectrodes fabricated *via* laser-pulling offer stable voltammetric responses for ferrocene oxidation in acetonitrile after CV cycling between +800 mV and -800 mV *vs.* Ag/AgCl (Figure 18a). However, pulled and etched nanoelectrodes are often recessed following polishing or exposure to solvent conditions [209, 218]. Steady-state voltammetric response with a smaller apparent electrode radii when assuming an inlaid disk geometry, a feature that cannot be detected or characterized solely by cyclic voltammetry.

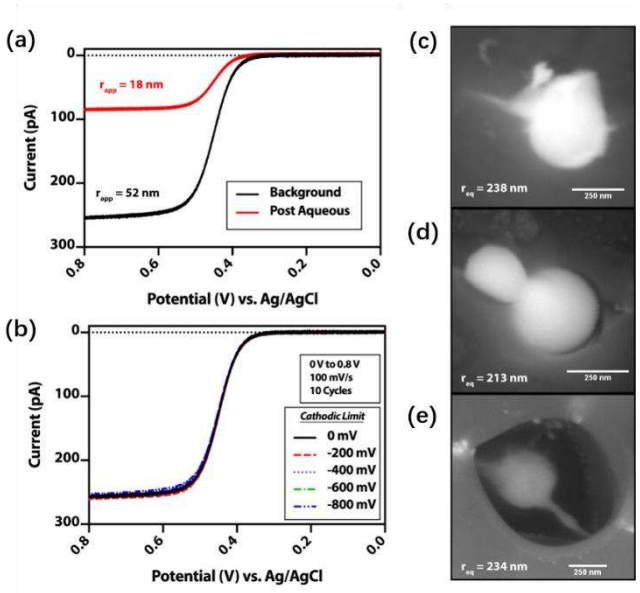

Figure 18. Nanoelectrode Stability. (a) Cyclic voltammogram of r_{app} 52 nm inlaid disk Pt nanoelectrode in 5 mM ferrocene in acetonitrile (black) with subsequent recession by ~85 nm following exposure to aqueous conditions, resulting in voltammogram corresponding to an r_{app} 18 nm Pt nanoelectrode. (b) Cyclic voltammogram of r_{app} 150 nm inlaid disk Pt nanoelectrode in 5 mM ferrocene in acetonitrile cycling between 0 to 0.8 V vs. Ag/AgCl following cycling between 0.8 V and cathodic limit for 10 cycles, demonstrating minimal variation in apparent radius between subsequent voltammetric cycling. (c) SEM characterization of inlaid disk Pt nanoelectrode with an equivalent radius of 238 nm with subsequent remounting in SEM (d) and *in situ* exposure to 100 µL acetonitrile (e) demonstrating significant variations in NP topography and the emergence of characteristic nanoelectrode recession following electron beam exposure under grounded conditions.

Analytical solutions for diffusion in a recessed nanoelectrode can be used to ensure that measurements at these electrodes is physically meaningful, however, the apparent radius will be consistently underreported if an inlaid disk geometry is assumed without verification *via* SEM, TEM, or AFM. Additionally, the geometry of an otherwise well characterized electrode can change rapidly following exposure to new conditions, as emphasized in Figure 18(b) demonstrating the change in steady-state current for ferrocene oxidation in acetonitrile after the electrode was dipped in deionized water for less than five seconds, corresponding to an apparent recession of ~85 nm. Furthermore, SEM characterization of these nanoelectrodes suggests that the exposed Pt surface is sensitive to handling and exposure to solvent under grounded conditions, as illustrated by the change in topography and equivalent radii in Figure 18(c-e). As the stability of nanoelectrodes under a wide range of solvent conditions, namely high cathodic potentials and aqueous solutions, have not yet been thoroughly examined, extensive care should be taken to verify nanoelectrode fidelity through the course of measurements, particularly at the single entity domain where variations in analyte flux profiles are accentuated between an ideal and a geometrically uncertain electrode, or when measuring electron transfer kinetics.[219]

6.4 Electron transfer at individual geometrical line interfaces

Coupled electron- and phase-transfer (CEPhT) reactions play a key role in many electrochemical systems, especially within energy conversion and storage technology. For example, during the intercalation of Li^+ in lithium-ion batteries, the Li^+ must cross from the liquid electrolyte phase into the electrode material concurrently with an electron transfer process, where the electrode material is oxidized or reduced. In a similar fashion, CEPhT reactions are also observed during electrodeposition, where the redox species transfers from a liquid phase to a solid phase while being oxidized or reduced. Furthermore, CEPhT reactions are essential in multiphase organic electrosynthesis,[220] which has been shown to be an environmentally friendly, economical, and safe alternative to homogeneous organic electrosynthesis. Multiphase electrosynthesis relies on the use of three immiscible phases, such as an electrode placed in an oil-in-water emulsion. These multiphase syntheses generally involve a CEPhT reaction, where either the reactant, product, intermediate, mediator or catalyst will undergo a phase-transfer coupled to an electron-transfer. In these examples, the three-phase interface is generally not geometrically well defined, making the mechanism of the reaction difficult to probe. For this reason, fundamental understanding of CEPhT reactions has been limited. To obtain insights into the kinetics, energetics, and mechanism involved in CEPhT reactions, a cylindrical wire electrode was placed across the interface of two immiscible liquids, creating a geometrically well-defined, three-phase interface of nanometer thickness [221, 222]. This system allows for a more precise study of CEPhT reactions that can be computationally modeled with relative ease.

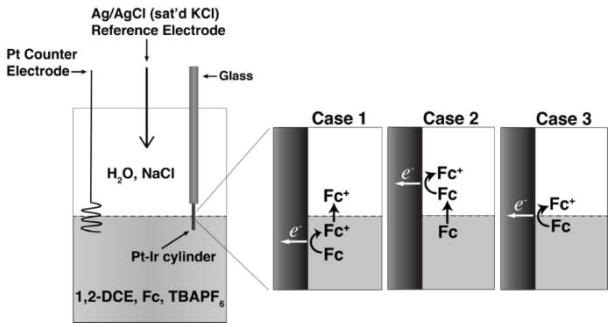

Figure 19 Schematic of the electrochemical cell used to probe CEPhT reactions. A 0.25 mm diameter Pt-Ir wire is placed across the DCE/H_2O interface, with the DCE phase containing TBAPF6 and Fc and the H_2O phase containing NaCl. The right-side diagram shows the possible mechanisms of a CEPhT reaction. Reproduced from ref. [223], copyright 2019 by the American Chemical Society.

The schematic in Figure 19 shows a Pt-Ir cylindrical wire across a 1,2-dichloroethane (DCE)/H_2O interface, where both liquid phases contained electrolyte, and the redox species ferrocene (Fc) was initially present only in the DCE. As shown in Figure 19, the CEPhT reaction can happen by three

mechanisms: the electron transfer step either preceding (case 1) or following (case 2) the phase transfer, or in a concerted mechanism, where the electron-transfer occurs concurrently with the phase transfer and no stable population of reaction intermediates is produced (case 3). Voltammetric characterization can experimentally distinguish between these three possible CEPhT mechanisms. Figure 20(a) shows two control experiments where the Pt-Ir wire was placed in the H_2O phase (red) and the DCE phase (black). No faradaic current is observed with the Pt-Ir wire in the H_2O phase as Fc is not soluble enough in H_2O to be electrochemically observed. When the Pt-Ir wire is placed in the DCE phase a voltammetric wave is seen corresponding to the oxidation and reduction of Fc present in that phase. Figure 20(b) shows the voltammetric response with the Pt-Ir wire placed across the DCE/H_2O interface. A similar response to the black curve in Figure 20(a) is observed, but two extra peaks are seen at lower potentials. After the initial oxidation of Fc in the DCE phase at ~0.63 V vs Ag/AgCl, the charged Fc product (Fc^+) produced near the three-phase interface transfers into the H_2O phase, due to its higher solubility in that phase. On the reverse scan of the first cycle, two reduction peaks are observed at 0.53 V and 0.28 V for the reduction of Fc^+ in DCE and H_2O, respectively. On the second cycle, Fc is present in both phases and oxidative peak currents are seen for the reaction in H_2O at 0.38 V and DCE at 0.63 V. Continuous cycling produces a steady-state response qualitatively similar to the second cycle in Figure 20(b).

Further experiments using this setup, determined the CEPhT reaction to be highly dependent on the three-phase interface geometry, and electrolyte concentration. It was also determined that the difference in ΔG for the Fc/Fc^+ reaction in the DCE and H_2O phases, was ~24 kJ/mol and that the rate of the CEPhT reaction is dominated by mass transport. This experimental design, combined with computational modeling, provides detailed insights into the mechanisms, energetics, and kinetics of CEPhT reactions, and could be used to elucidate these details in other chemical systems.

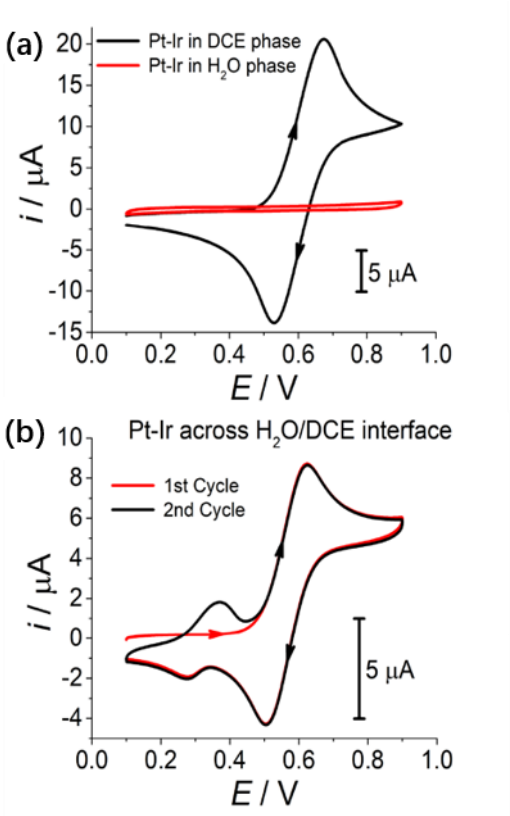

Figure 20 Cyclic voltammetry corresponding to the Pt-Ir wire electrode positioned at different locations relative to the H_2O/DCE interface. (a) The voltammetric response with Pt-Ir placed completely in the DCE phase (black), and the Pt-Ir electrode fully emerged in the H_2O phase (red). (b) The voltammetric response with the Pt-Ir electrode placed across the H_2O/DCE interface. Reproduced from ref. [223], copyright 2019 by the American Chemical Society.

6.5 Imaging buried interfaces

The development of electrochemical microscopy techniques paves a new way to precisely understand chemical process at single-entity level in confined spaces.[224] After three decades of development, SECM has been shown to be powerful as a means for measuring numerous surface electrochemical properties, but the drawbacks often limit its capability in a number of applications. For example, the entire sample needs to be immersed in electrolyte, which makes it challenging for single-entity measurements. The recent introduction of scanning electrochemical cell microscopy (SECCM) is a significant advancement augmenting the capabilities of electrochemical microscopy.[225] In contrast to the solid metal electrodes typically used as the probe in SECM, the probe in SECCM is a micro-/nanopipette filled with electrolyte solution. A cell is formed by the meniscus at the end of the pipette in contact with the sample surface, which allows for highly localized electrochemical measurements. This technique is very useful for studying ion transfer reactions, phase transformations, and correlating electrochemical properties with topographical features, including localized activity variation

on single entitles, such as nanoparticles, nanotubes, and electrocatalysis at grain boundaries [226-228].

SECCM is anticipated to help address practical problems in functioning systems; for instance, through quantifying the kinetics of ion transfer at interfaces, which is an extremely important parameter in energy storage. However, it is difficult to detect the ion transfer and understand the factors influencing ion transfer at buried electrode/electrolyte interfaces, due to the lack of *operando* electrochemical methods with nanoscale resolution. Recently, a voltammetric SECCM method was employed for the electrochemical interrogation of hydrogen evolution reaction (HER) at the buried interface in a model fuel cell cathode. As shown in Figure 21(a), Pt nanoparticles (PtNPs) are deposited on highly oriented pyrolytic graphite (HOPG) surface and covered by a Nafion nanofilm as a proton exchange membrane; the Nafion-PtNPs interfaces constitutes a buried interface. Using SECCM, the localized HER activity of HOPG, Nafion/HOPG, and PtNPs underneath Nafion can be readily distinguished via their voltammograms. Owing to the kinetics of HER on Pt being significantly faster than that on the other sites, it has a highest current enhancement in the voltammogram (Figure 21(b)). The electrochemical behavior of the scanned region can also be visualized by an equipotential map, which is formed by extracting a single current from the voltammogram at each site. As shown in Figure 21(c), the equipotential map not only shows the current enhancement of each site, but also describe the size of buried PtNPs. SECCM further revealed variation in the HER activity with changing the thickness of the buried interface. The activity current enhancement rose first and then declined as the Nafion film thicknesses was increasing from 80 nm to 800 nm, and the optimized current enhancement occurred on 200 nm Nafion film. This trend is attributed to the balance among the ion concentration enrichment, water content fluctuation, and the restriction for proton transport in Nafion.

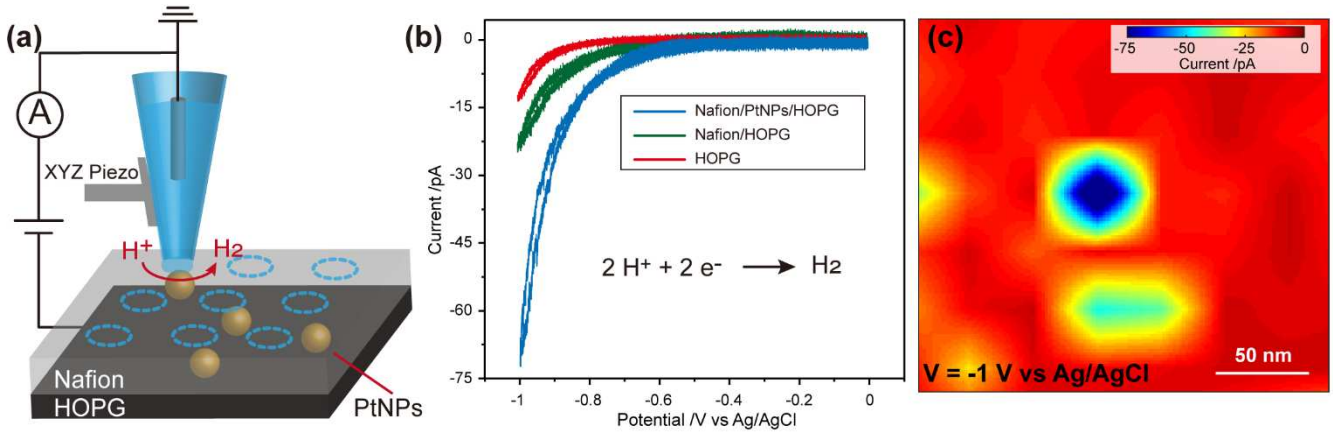

Figure 21 Visualizing proton reduction on 35-nm radius Pt nanoparticles buried in a 150-nm thick Nafion film (a) Schematic of SECCM measurement. (b) Voltammetry of HER on HOPG (red), Nafion/HOPG surface (green), and Nafion/PtNP/HOPG (blue). (c) Electrochemical image (121 pixels over a 200 × 200 nm scan area at -1 V vs Ag/AgCl.). The 100 nm-diameter nanopipette contained 25 mM $HClO_4$; ν = 0.1 V/s.

7. Perspective

In this review, we have summarized recent developments in the single entity electrochemistry. The overall motivation of single entity electrochemistry is to learn new chemical knowledge based on measurements of single molecules, single nanoparticles, single cells and even single tissues. Using nanoscale sensing interfaces, single entity electrochemistry exhibits high spatial resolution, high temporal resolution and feasible combination with other techniques. Therefore, the single entity electrochemistry is being widely employed in biosensing, early disease diagnostics and prewarning, exploring the mechanisms for energy transformation, revealing the catalysis activities and pathogenic studies. Despite the significant progresses in developing the suitable sensing interfaces and novel sensing mechanisms for single entity electrochemistry, this field is still in a phase of rapid growth and discovery. We end our review here by discussing some of the scientific challenges to be conquered while proposing some additional areas for future work.

In the field of single molecule detection, the single-biomolecule interface provides unprecedented spatiotemporal resolution for single molecule sensing, allowing sufficient observation time for each analyte and higher throughput recording mode. However, most of nanopore-based single molecule studies are focused on the pure samples and artificial system instead of applying into the real biosystems. Driven by the motivation for exploring the biological crosstalk, the nanopore-based single molecule tool needs directly to acquire electrochemical signal containing single molecule information from the single cells. The possible solution is to combine the pore forming biomolecules with nanopipette structure. Such powerful single molecule sensor could be used to

monitor single-molecule biological processes in vivo. Moreover, the robustness of these sensors should be enhanced to withstand the harsh real sample condition, and the selectivity should be improved to meet the requirement in simultaneous identification and quantitation of difference species *in vivo*. Then, the corresponding data analysis algorithm should be developed to uncover the interaction and kinetics of single molecules in biological crosstalk. The possibility of controlling the electrokinetics inside a nanopipette-biological nanopore hybrid system could be useful to meet the low detection limit in vivo sensing.

For the single nanoparticle detection, the following efforts are still needed from both activity measurement and structure characterization before single nanoparticle electrochemistry can reach its ultimate goal on the bottom-up SAR. First, intra-nanoparticle features such as facets and defects often play critical roles in regulating the activity of single nanoparticles. It thus requires a capability to map the sub-nanoparticle-level distribution of electrochemical reactivity inside a single nanoparticle. Many concepts originated from super-resolved fluorescence microscopy, such as super-localization and optical reconstruction, are anticipated to improve the spatial resolution of optical electrochemical imaging[112, 113, 229] Second, activity measurement has so far been limited under constant potential (for collision) and potential sweeping conditions (for scanning electrochemical imaging and optical electrochemical imaging). Despite of the critical roles of impedance measurements in traditional electrochemistry, efforts on single nanoparticle impedance spectroscopy are still rare. [118] The incorporation of temporal (frequency) dimension in impedance spectroscopy should provide valuable information to decouple multiple electron transfer processes including electrode-nanoparticle contacts, double-layer charging, ionic migration and electron hopping within the nanoparticles. From another aspect, great efforts are also demanded to improve the capability for *in situ* characterizing the structural feature of single nanoparticles. Scanning electron microscopes are the most feasible techniques so far to access the size and morphology, which, however, often exhibited weak correlation with the activity due to the lack of internal information such as crystallinity, atomic arrangement and defects. We expected the adoption of more techniques, such as high resolution transmission electron microscopy and transmission X-ray microscopy, to comprehensively characterize the internal structure of single nanoparticles. Energy spectroscopy and optical spectroscopy are anticipated to play more important roles in resolving the chemical states of single nanoparticles. Once the activity and structural of single nanoparticles can be comprehensively and reliably determined, it would be natural for single nanoparticle electrochemistry to build a bottom-up methodology to uncover the SAR, and to guide the rational design of electroactive nanomaterials with better performance.

In single cell analysis, nanoscale devices capable of single-cell extraction and analysis have thus far been used only in proof of concept studies, this presents a huge arena of biological questions such techniques could be employed to answer in the future. The concept of single-cell nanosurgery relies on the fact that intracellular contents cannot be measured in situ (i.e., within the intracellular environment) so that the analyte of interest needs to be first extracted and then, often after amplification, analysed ex-situ with state of the art techniques, like next-generation sequencing of mass spectrometry. This is not the case for every intracellular molecule and with the development of reproducible fabrication methods for nanoelectrodes a number of redox active molecules can be detected and quantified within the cell of interest. For example, Ying et al have reported an elegant signal amplification approach where only the inner walls of a quartz nanopipette were coated with Au[230]. Upon functionalization of the gold layer with catechol the nanoelectrode showed a remarkable sensitivity to redox-active species like NADH. The authors explain the enhanced sensitivity due to the generation of H_2 nanobubbles at the nanopipette tip. Remarkably, the authors also showed the ability of this nanoelectrode system to detect redox active species within a single living cell. Platinised carbon nanoelectrodes have been used extensively for the detection of reactive oxygen and nitrogen species in single cells and the groups led by Amatore, Mirkin and Ewing amongst others have demonstrated the potential of this technique for quantitative intracellular measurement and recently even within cellular vesicles like lysosomes[231, 232]. Also, there is a great potential for single molecule entity manipulation within living cells as recently demonstrated with nanopore and nanoelectrode-based platforms to enable perturbation and monitoring of living cells with high spatial and temporal resolution[134, 139, 233]. As thus far nanoscale devices capable of single-cell extraction and analysis have been used only in proof of concept studies, this presents a huge arena of biological questions such techniques could be employed to answer in the future.

The unremitting development of electrochemical measurements is expected to address the challenge of precisely describing complex electrochemical mechanisms in multiple phases at a confined space. For example, the measurement of critical nucleation parameters demands highly sensitive and rapid detection because of the nuclei nanoscopic size and the unstable kinetics. The introduction of nanoelectrodes provides a confined area to precisely study this process with a high temporal resolution and repeatability. CEPhT is another challenging scenario happening at all multiple phases in electrochemistry. Taking advantage of the nanopipette based electrochemical approaches, the dimension of the reaction zone is expected to be precisely characterized. The role of crystallinity and grain boundaries in influencing electrochemical ion transfer rates at the buried interface, battery structure is still largely unexplored, due to the lack of *operando* methods for probing buried interfaces with nanoscale resolution. The use of SECCM is expected to advance the study of ion transfer reactions and phase transformations at buried interfaces in energy storage with a high spatial resolution. There measurements will make a significant contribution to material, energy, physics as well as chemistry by

yielding experimental kinetic rate parameters that test theoretical predictions.

Undoubtedly, the single-entity electrochemistry pushes the forefront of our ability to make analytical measurements. The further development of advance instrumentation with high spatial and temporal resolution, new theory for nanoelectrochemistry and new sensing mechanisms, will further facilitate the application of single-entity electrochemistry.

Acknowledgments

Yi-Tao Long would like to acknowledge funding from National Natural Science Foundation of China (21834001) and the Excellent Research Program of Nanjing University (ZYJH004). Yi-Lun Ying is sponsored by National Ten Thousand Talent Program for young top-notch talent. Jiajun Wang is sponsored by National Natural Science Foundation of China (61901171).

Wei Wang would like to acknowledge funding from National Natural Science Foundation of China (21925403 and 21874070).

Paolo Actis would like to acknowledge funding from the European Union's Horizon 2020 research and innovation programme under the Marie Skłodowska-Curie grant agreement No 812398.

Lanqun Mao would like to acknowledge funding supported by the National Natural Science Foundation of China (21790390, 21790391), the Strategic Priority Research Program of Chinese Academy of Sciences (XDB30000000), the National Basic Research Program of China (2018YFE0200800, 2018YFA0703501 and 2016YFA0200104), and the Chinese Academy of Sciences (QYZDJ-SSW-SLH030).

Henry White would like to acknowledgment funding from Office of Naval Research (N00014-19-1-2331), the US Air Force Office of Scientific Research MURI (FA9550-14-1-0003) and by the Nanostructures for Electrical Energy Storage (NEES), an Energy Frontier Research Center funded by the US Department of Energy, Office of Science, and Basic Energy Sciences under Award number DESC0001160. The images reported in Figure 21 (b) were acquired using instrumentation purchased with support from the Office of Naval Research DURIP program (N00014-18-1-2235).

Conflict of interest The authors declare that they have no conflict of interest.

Author Contributions Section 1 is contributed by all authors. Section 2 is contributed by Y-T. L., J.W. and Y-L., Y. Section 3 is contributed by W.W., Section 4 is contributed by A. R. L and P A, Section 5 is contributed by Y. J., C. X. and L. M., Section 6 is contributed by R. G., M. A. E., A. D. P., H. R., C. K. T. W., and H. S. W., and Section 7 is contributed by all authors.

References

1. Baker, L.A., *J Am Chem Soc*, 2018. **140**(46): p. 15549-15559.

2. Long, Y.T., P.R. Unwin, and L.A. Baker, *ChemElectroChem*, 2018. **5**(20): p. 2918-2919.

3. Gooding, J.J. and K. Gaus, *Angew Chem Int Ed*, 2016. **55**(38): p. 11354-11366.

4. Wu, Y., R.D. Tilley, and J.J. Gooding, J *J Am Chem Soc* , 2019. **141**(3): p. 1162-1170.

5. Ying, Y.-L. and Y.-T. Long, *J Am Chem Soc* , 2019. **141**(40): p. 15720.

6. Shi, W., A.K. Friedman, and L.A. Baker, *Anal. Chem*, 2016. **89**(1): p. 157-188.

7. Mirkin, M.V., et al., *Acc Chem Res* , 2016. **49**(10): p. 2328-2335.

8. Fu, K. and P.W. Bohn, *ACS Cent Sci*, 2018. **4**(1): p. 20-29.

9. Allerston, L.K. and N.V. Rees, *Curr Opin in Electrochemistry.* 2018. **10**: p. 31-36.

10. Bentley, C.L., M. Kang, and P.R. Unwin, *J Am Chem Soc* , 2019. **141**(6): p. 2179-2193.

11. Anderson, T.J. and B. Zhang, *Acc Chem Res*, 2016. **49**(11): p. 2625-2631.

12. Kleijn, S.E.F., et al., *Angew Chem Int Ed*, 2014. **53**(14): p. 3558-3586.

13. Valenti, G., et al., *J Am Chem Soc*, 2017. **139**(46): p. 16830-16837.

14. Lugo-Morales, L.Z., et al. *Anal. Chem*, 2013. **85**(18): p. 8780-8786.

15. Wang, W., *Chem Soc Rev.*, 2018. **47**(7): p. 2485-2508.

16. Harrison, A.G., *Chemical ionization mass spectrometry*. 2018: Routledge.

17. Li, H., et al., Sensors, 2017. **17**(1): p. 74.

18. Kranz, C., *Faraday Discuss* 2018. **210**: p. 499-501.

19. Crooks, R.M., *Faraday Discuss* , 2016. **193**: p. 533-547.

20. Ying, Y.-L., et al., *Nat Sci Rev* , 2018. **5**(4): p. 450-452.

21. Meller, A., *Nature Nanotechnol*, 2019. **14**(8): p. 732-733.

22. Howorka, S. and Z. Siwy, *Chem Soc Rev* , 2009. **38**(8): p. 2360-2384.

23. Venkatesan, B.M. and R. Bashir, *Nature Nanotechnol* , 2011. **6**(10): p. 615.

24. Ying, Y.-L., et al., *Angew Chem Int Ed* , 2013. **52**(50): p. 13154-13161.

25. Deamer, D., M. Akeson, and D. Branton, *Nature biotechnol*, 2016. **34**(5): p. 518.

26. Restrepo-Perez, L., C. Joo, and C. Dekker, *Nature Nanotechnol* , 2018. **13**(9): p. 786-796.

27. Luchian, T., et al., *Acc Chem Res*, 2019. **52**(1): p. 267-276.

28. Luo, L., et al., *Annu Rev Anal Chem*, 2014. **7**: p. 513-535.

29. Cao, C. and Y.-T. Long, *Acc Chem Res* , 2018. **51**(2): p. 331-341.

30. Yu, R.J., et al., *Angew Chem Int Ed* , 2018, **58**(12): p.3706

31. Patrice, F.T., et al., *Annu Rev Anal Chem, Vol 12*, P.W. Bohn and J.E. Pemberton, Editors. 2019. p. 347-370.

32. Liu, S.-C., et al., *Faraday Discuss*, 2018. **210**(0): p. 87-99.

33. Wang , J., et al., *Chem Asian J* , 2019. **14**(3): p. 389-397.

34. Kasianowicz, J.J., et al., *Proc Natl Acad Sci U S A* , 1996. **93**(24): p. 13770.

35. Song, L., et al., *Science*, 1996. **274**(5294): p. 1859.

36. Iacovache, I., et al., *Nat Commun*, 2016. **7**(1): p. 12062.

37. Faller, M., M. Niederweis, and G.E. Schulz, *Science*, 2004. **303**(5661): p. 1189.

38. Subbarao, G.V. and B. van den Berg, *J Mol Biol* , 2006. **360**(4): p. 750-759.

39. Cao, B., et al., *Proc Natl Acad Sci U S A* , 2014. **111**(50): p. E5439.

40. De Colibus, L., et al., *Structure*, 2012. **20**(9): p. 1498-1507.

41. Locher, K.P., et al., *Cell*, 1998. **95**(6): p. 771-778.

42. Bräuning, B., et al., *Nat Commun*, 2018. **9**(1): p. 1806.

43. Simpson, A.A., et al., *Nature*, 2000. **408**(6813): p. 745-750.

44. Sun, K., et al., *Nat Commun*, 2019. **10**(1): p. 5083.

45. Montal, M. and P. Mueller, *Proc Natl Acad Sci U S A* , 1972. **69**(12): p. 3561.

46. Wu, X.-Y., et al., *J Chin Chem Soc-Taip,* 2019. **1**(3): p. 304.

47. Li, M.-Y., et al., *Front Chem*, 2019. **7**: p. 528.

48. Wang, Y.-Q., et al., *Anal. Chem* , 2018. **90**(13): p. 7790-7794.

49. Cao, C., et al., *Nat Protoc*, 2017. **12**: p. 1901.

50. Wang, J., et al., *Angew Chemie Int Ed,* 2020. DOI: 10.1002/anie.201913618

51. Goodwin, S., J.D. McPherson, and W.R. McCombie, *Nat Rev Gene* , 2016. **17**(6): p. 333.

52. Brown, C.G. and J. Clarke, *Nat Biotechnol*, 2016. **34**(8): p. 810.

53. Jain, M., et al., *F1000Res*, 2017. **6**. doi: 10.12688/f1000research

54. Jin, Q., et al., *J Am Chem Soc* , 2013. **135**(51): p. 19347-19353.

55. Schibel, A.E.P., et al., *J Am Chem Soc* , 2010. **132**(51): p. 17992-17995.

56. Zhang, J.H., et al., *Chem Commun (Camb)*, 2017. **53**(73): p. 10176-10179.

57. Tian, K., et al., *ACS Nano*, 2013. **7**(5): p. 3962-3969.

58. Zhang, X., et al., *Nat Commun*, 2017. **8**(1): p. 1458.

59. Sheng, Y., et al., *Analyst*, 2018. **143**(10): p. 2411-2415.

60. Ramsay, W.J. and H. Bayley, Angew Chem Int Ed , 2018. **57**(11): p. 2841-2845.

61. Lu, Y., et al., *Chem Commun (Camb)*, 2019. **55**(63): p. 9311-9314.

62. Hu, Z.L., et al., *Anal Chem*, 2018. **90**(7): p. 4268-4272.

63. Cao, C., et al., *Nat Nanotechnol*, 2016. **11**(8): p. 713-8.

64. Zeng, T., et al., *Biochemistry*, 2017. **56**(11): p. 1596-1603.

65. Wang, H.Y., et al., *Anal Chem*, 2013. **85**(17): p. 8254-61.

66. Qing, Y., et al., *Science*, 2018. **361**(6405): p. 908-912.

67. Lieberman, K.R., et al., *J Am Chem Soc* , 2010. **132**(50): p. 17961-17972.

68. Stefureac, R., et al.,. *Biochemistry*, 2006. **45**(30): p. 9172-9179.

69. Long, Y. and M. Zhang,. *Sci. China Ser. B-Chem* , 2009. **52**(6): p. 731-733.

70. Houghtaling, J., J. List, and M. Mayer, *Small*, 2018. **14**(46): p. 1802412.

71. Wang, H.-Y., et al., *Anal. Chem* , 2011. **83**(5): p. 1746-1752.

72. Liao, D.-F., et al., *Small*, 2018. **14**(18): p. 1704520.

73. Asandei, A., et al., *J Membr Biol*, 2014. **247**(6): p. 523-530.

74. Li, S., et al., *ChemElectroChem*, 2019. **6**(1): p. 126-129.

75. Piguet, F., et al., *Nat Commun*, 2018. **9**(1): p. 966.

76. Huang, G., A. Voet, and G. Maglia, *Nat Commun*, 2019. **10**(1): p. 835.

77. Ionescu, S.A., et al., *ChemBioChem*, 2017. **18**(6): p. 554-562.

78. Liu, L., et al., *ACS Sens*, 2019. **4**(5): p. 1323-1328.

79. Borsley, S. and S.L. Cockroft, *ACS Nano*, 2018. **12**(1): p. 786-794.

80. Ying, Y.-L., et al., *Research*, 2019. **2019**: p. 1050735..

81. Rosen, C.B., D. Rodriguez-Larrea, and H. Bayley, *Nat Biotechnol*, 2014. **32**(2): p. 179.

82. Harrington, L., et al., *ACS Nano*, 2019. **13**(1): p. 633-641.

83. Willems, K., et al., *Phil. Trans. R. Soc. B* 2017. **372**(1726): p. 20160230.

84. Zhao, Q., et al., *J Am Chem Soc* , 2009. **131**(18): p. 6324-6325.

85. Cao, C., et al., *Nat Commun*, 2018. **9**(1): p. 2823.

86. Wang, J., et al., *ACS Cent Sci*, 2020, DOI: 10.1021/acscentsci.9b01129

87. Zhou, B., et al., *Sci. China Chem* , 2018, 61: p. 1385

88. Manrao, E.A., et al., *Nat Biotechnol,* 2012. **30**(4): p. 349-353.

89. Wang, J., et al., *Angew Chem Int Ed* , 2019. **58**(14): p. 4737-4741.

90. Li, Y., J.T. Cox, and B. Zhang, *J Am Chem Soc* , 2010. **132**(9): p. 3047-3054.

91. Hua, H., et al., *Anal. Chem* , 2018. **90**(16): p. 9677-9681.

92. Aiyappa, H.B., et al., *Angew Chem Int Ed* , 2019. **58**(26): p. 8927-8931.

93. Quinn, B.M., P. van 't Hof, and S.G. Lemay, *J Am Chem Soc* , 2004. **126**(27): p. 8360-8361.

94. Gao, G., et al., *Anal. Chem* , 2018. **90**(20): p. 12123-12130.

95. Dick, J.E., et al., *Proc Natl Acad Sci U S A* , 2016. **113**(23): p. 6403-6408.

96. Xiao, X. and A.J. Bard, *J Am Chem Soc* , 2007. **129**(31): p. 9610-+.

97. Peng, Y.-Y., et al., *Angew Chem Int Ed* , 2018. **57**(14): p. 3758-3762.

98. Ma, H., et al., *J Am Chem Soc* , 2018. **140**(15): p. 5272-5279.

99. Zhou, Y.-G., N.V. Rees, and R.G. Compton, *Angew Chem Int Ed* , 2011. **50**(18): p. 4219-4221.

100. Evers, M.V., et al., *Angew Chem Int Ed*, 2019. **58**(24): p. 8221-8225.

101. Sun, L., et al., *Anal. Chem* , 2017. **89**(11): p. 6051-6056.

102. Li, X., et al., *Angew Chem Int Ed* , 2015. **54**(41): p. 11978-11982.

103. Cheng, W. and R.G. Compton, *Angew Chem Int Ed* , 2014. **53**(50): p. 13928-13930.

104. Sun, T., et al., *Angew Chem Int Ed* , 2014. **53**(51): p. 14120-14123.

105. Tao, B., et al., *Angew Chem Int Ed* , 2019. **58**(14): p. 4606-4611.

106. Sun, L., et al., *Nano Res*, 2017. **10**(5): p. 1740-1748.

107. Brasiliense, V., et al., *J Am Chem Soc* , 2016. **138**(10): p. 3478-3483.

108. Evans, R.C., et al., *Proc Natl Acad Sci U S A* , 2019. **116**(26): p. 12666-12671.

109. Hill, C.M. and S. Pan, *Proc Natl Acad Sci U S A* , 2013. **135**(46): p. 17250-17253.

110. Fang, Y., et al., *Proc Natl Acad Sci U S A* , 2014. **136**(36): p. 12584-12587.

111. Nizamov, S., O. Kasian, and V.M. Mirsky, *Angew Chem Int Ed* , 2016. **55**(25): p. 7247-7251.

112. Xu, W., et al., *Nano Lett*, 2009. **9**(12): p. 3968-3973.

113. Wilson, A.J. and K.A. Willets,. *Nano Lett*, 2014. **14**(2): p. 939-945.

114. Zhu, M.-J., et al., *Angew Chem Int Ed* , 2018. **57**(15): p. 4010-4014.

115. Shan, X., et al., *Nat Nanotechnol*, 2012. **7**(10): p. 668-672.

116. Jiang, D., et al., *J Am Chem Soc* , 2017. **139**(1): p. 186-192.

117. Novo, C., et al., *J Am Chem Soc* , 2009. **131**(41): p. 14664

118. Liu, T., et al., *Chem Sci*, 2018. **9**(19): p. 4424-4429.

119. Wang, H., et al., *Nano Lett*, 2017. **17**(1): p. 236-241.

120. Xia, Q., et al., *Nat Commun*, 2019. **10**(1): p. 3849-3849.

121. Hooke, R., ed. *Micrographia: or some physiological descriptions of minute bodies made by magnifying glasses. : With observations and inquiries thereupon*. Vol. . 1665, Jo. Martyn, and Ja. Allestry: London.

122. Ribatti, D.,. *Exp Cell Res*, 2018. **364**(1): p. 1-4.

123. Actis, P., *Small Methods*, 2018. **2**(3), p.1700300.

124. Espina, V., et al., *Nat Protoc*, 2006. **1**(2): p. 586-603.

125. Battich, N., T. Stoeger, and L. Pelkmans,. *Nat Methods*, 2013. **10**(11): p. 1127-1133.

126. Zare, R.N. and S. Kim, Annu Rev Biomed Eng , Vol 12, 2010. **12**: p. 187-201.

127. Prakadan, S.M., A.K. Shalek, and D.A. Weitz, *Nature Reviews Genet*, 2017. **18**(6), p. 345

128. Sarkar, A., et al., *Nat Commun*, 2014. **5**, p. 3421

129. Higgins, S.G. and M.M. Stevens, *Science*, 2017. **356**(6336): p. 379-380.

130. Nawarathna, D., T. Turan, and H.K. Wickramasinghe, *Appl Phys Lett.* , 2009. **95**(8).

131. Nawarathna, D., et al., *Anal Biochem*, 2011. **408**(2): p. 342-4.

132. Tao, Y.L. and H.K. Wickramasinghe, *Appl Phys Lett.*, 2017. **110**(7).

133. Li, X., et al., *Lab Chip*, 2017. **17**(9): p. 1635-1644.

134. Nadappuram, B.P., et al., *Nat Nanotechnol*, 2019. **14**(1): p. 80-88.

135. McKelvey, K., et al., *Anal Chem,* 2013. **85**(15): p. 7519-26.

136. Guillaume-Gentil, O., et al., *Trends Biotechnol*, 2014. **32**(7): p. 381-8.

137. Guillaume-Gentil, O., et al., *Cell*, 2016. **166**(2): p. 506-16.

138. Guillaume-Gentil, O., et al., *Anal Chem*, 2017. **89**(9): p. 5017-5023.

139. Aramesh, M., et al., *Nat Nanotechnol*, 2019.

140. Actis, P., et al., *ACS Nano*, 2014. **8**(1): p. 546-53.

141. Chen, C.C., Y. Zhou, and L.A. Baker, *Annu Rev Anal Chem (Palo Alto Calif),* 2012. **5**: p. 207-28.

142. Novak, P., et al., *Nat Methods*, 2009. **6**(4): p. 279-281.

143. Rheinlaender, J., et al., *Langmuir*, 2011. **27**(2): p. 697-704.

144. Actis, P., A.C. Mak, and N. Pourmand, *Bioanal Rev*, 2010. **1**(2-4): p. 177-185.

145. Laforge, F.O., et al., *Proc Natl Acad Sci U S A* , 2007. **104**(29): p. 11895-11900.

146. Toth, E.N., et al., *J Biol Chem*, 2018. **293**(13): p. 4940-4951.

147. Nashimoto, Y., et al., *ACS Nano*, 2016. **10**(7): p. 6915-6922.

148. Nashimoto, Y., et al., *Anal Chem*, 2019. **91**(14): p. 8772-8776.

149. Saha-Shah, A., et al., *Analyst*, 2016. **141**(6): p. 1958-1965.

150. Yin, R., V. Prabhakaran, and J. Laskin, *Anal Chem*, 2018. **90**(13): p. 7937-7945.

151. Cao, Y.H., et al., *Proc Natl Acad Sci U S A,* 2017. **114**(10): p. E1866-E1874.

152. VanDersarl, J.J., A.M. Xu, and N.A. Melosh, *Nano Lett.,* 2012. **12**(8): p. 3881-3886.

153. Xu, A.M., et al., *Nat Commun*, 2014. **5**.

154. Singhal, R., et al., *Nat Nanotechnol*, 2011. **6**(1): p. 57-64.

155. Yan, R., et al., *Nat Nanotechnol,* 2011. **7**(3): p. 191-6.

156. Zhang, M., et al., *Anal. Chem* , 2005. **77**(19): p. 6234-6242.

157. Hou, H., et al., *Sci China Chem*, 2019: p. 1-5.

158. Cheng, H., X. Wang, and H. Wei, *Anal. Chem* , 2015. **87**(17): p. 8889-8895.

159. Zhuang, X., et al., *Anal. Chem*, 2012. **84**(4): p. 1900-1906.

160. Zhang, L., et al., *Anal. Chem* , 2017. **89**(3): p. 1831-1837.

161. Yan, H., et al., *Angew Chem Int Ed,* 2018. **57**(15): p. 3922-3926.

162. Lin, Y., et al., *Anal. Chem*, 2009. **81**(6): p. 2067-2074.

163. Fan, Z., S. Guo-Yue, and T. Yang, Chinese J Anal Chem, 2019. **47**(3): p. 347-354.

164. Zhao, L., et al., *Anal. Chem*, 2019. **91**(7): p. 4421-4428.

165. Liu, J., *Nat Nanotechn*, https://doi.org/10.1038/s41565-020-0634-4.

165. Wu, F., et al., *Anal. Chem*, 2018. **90**(21): p. 13021-13029.

166. Xiao, T., et al., *Anal. Chem*, 2018. **90**(7): p. 4840-4846.

167. Schwerdt, H.N., et al., *Proc Natl Acad Sci U S A*, 2017. **114**(50): p. 13260-13265.

168. Ganesana, M., et al., Biosens Bioelectron, 2019. **130**: p. 103-109.

169. Xiao, T., et al., *Anal. Chem* , 2018. **90**(22): p. 13783-13789.

170. Smith, S.K., et al., ACS Chem Neurosci , 2017. **8**(2): p. 272-280.

171. Smith, S.K., et al., *Anal. Chem* , 2018. **90**(21): p. 12994-12999.

172. Zhang, Z., et al., *Analyst*, 2015. **140**(15): p. 5039-5047.

173. Llaudet, E., et al., *Anal. Chem* , 2005. **77**(10): p. 3267-3273.

174. Wang, S., X. Liu, and M. Zhang, *Anal. Chem*, 2017. **89**(10): p. 5382-5388.

175. Wang, K., et al., *Anal. Chem* , 2017. **89**(17): p. 9502-9507.

176. Xiao, T., et al., *Angew Chem Int Ed* , 2019. **131**(20): p. 6688-6691.

177. Xin, Y., et al., *Sci China Chem* , 2013. **56**(2): p. 256-261.

178. Fan, Y., C. Han, and B. Zhang, *Analyst*, 2016. **141**(19): p. 5474-5487.

179. Murray, R.W., *Chem Rev,* 2008. **108**(7): p. 2688-2720.

180. Conyers, J.L. and H.S. White, *Anal. Chem* , 2000. **72**(18): p. 4441-4446.

181. Zhang, B., Y. Zhang, and H.S. White, *Anal. Chem* , 2004. **76**(21): p. 6229-38.

182. Zhang, B., et al., *Anal. Chem*, 2007. **79**(13): p. 4778-4787.

183. Ma, W., et al., *Nano Lett*, 2017. **17**(7): p. 4354-4358.

184. Kai, T., C.G. Zoski, and A.J. Bard, *Chem Commun*, 2018. **54**(16): p. 1934-1947.

185. Bentley, C.L., M. Kang, and P.R. Unwin, *Curr Opin in Electrochemistry*, 2017. **6**(1): p. 23-30.

186. Ebejer, N., et al., *Annu Rev Anal Chem*, 2013. **6**: p. 329-351.

187. Seh, Z.W., et al., *Science*, 2017. **355**(6321): p. eaad4998.

188. Karlsson, R.K. and A. Cornell, *Chem Rev*, 2016. **116**(5): p. 2982-3028.

189. Kashchiev, D., *Nucleation: Basic Theory with Applications. Butterworth*. 2000, Heineman, Oxford.

190. Luo, L. and H.S. White, *Langmuir*, 2013. **29**(35): p. 11169-11175.

191. Chen, Q., et al., *J Phys Chem Lett* , 2014. **5**(20): p. 3539-3544.

192. Chen, Q., et al., *J Am Chem Soc* , 2015. **137**(37): p. 12064-12069.

193. Edwards, M.A., H.S. White, and H. Ren, *ACS Nano*, 2019. **13**(6): p. 6330-6340.

194. German, S.R., et al., *J Am Chem Soc* , 2018. **140**(11): p. 4047-4053.

195. German, S.R., et al., *ACS Nano*, 2015. **9**(7): p. 7186-7194.

196. Zhang, Y., et al., *J Phys Chem Lett C*, 2016. **120**(37): p. 20781-20788.

197. Edwards, M.A., et al., *ACS Nano*, 2015. **9**(12): p. 12274-12282.

198. German, S.R., et al., *J Phys Chem Lett C*, 2012. **117**(1): p. 703-711.

199. Qin, Z., J. Zhe, and G.-X. Wang,. *Meas Sci Technol* , 2011. **22**(4): p. 045804.

200. Ortega, A. and J. Garcıa de la Torre, *J Chem Phys*, 2003. **119**(18): p. 9914-9919.

201. Lan, W.J., et al., *J Phys Chem Lett C*, 2014. **118**(5): p. 2726-2734.

202. Han, C., et al., *Langmuir*, 2019. **35**(22): p. 7180-7190.

203. Holden, D.A., et al., *J Phys Chem C Nanomater Interfaces*, 2011. **115**(7): p. 2999-3004.

204. McKelvey, K., et al., *Curr Opin in Electrochemistry* , 2017. **6**(1): p. 4-9.

205. Yu, Y., et al., *ACS Nano*, 2017. **11**(10): p. 10529-10538.

206. Wang, Y., H. Cai, and M.V. Mirkin, *ChemElectroChem*, 2015. **2**(3): p. 343-347.

207. McKelvey, K., M.A. Edwards, and H.S. White, *J Phys Chem Lett* , 2016. **7**(19): p. 3920-3924.

208. Katemann, B.B. and W. Schuhmann, *Electroanalysis*, 2002. **14**(1): p. 22-28.

209. Bae, J.H., Y. Yu, and M.V. Mirkin,. *ChemElectroChem*, 2016. **3**(12): p. 2043-2047.

210. Duay, J., J.M. Goran, and K.J. Stevenson, *Anal. Chem* , 2014. **86**(23): p. 11528-11532.

211. Kim, J., et al., *J Am Chem Soc* , 2014. **136**(23): p. 8173-8176.

212. Jena, B.K., S.J. Percival, and B. Zhang, *Anal. Chem* , 2010. **82**(15): p. 6737-6743.

213. Hao, R. and B. Zhang, *Anal. Chem* , 2015. **88**(1): p. 614-620.

214. Yu, Y., et al., ChemElectroChem, 2015. **2**(1): p. 58-63.

215. Zhang, B., et al., *J Am Chem Soc* , 2013. **135**(27): p. 10073-10080.

216. Nioradze, N., et al., *Anal. Chem* , 2013. **85**(13): p. 6198-6202.

217. Sun, T., P.Y. Blanchard, and M.V. Mirkin, *Anal. Chem* , 2015. **87**(8): p. 4092-4095.

218. Nogala, W., J. Velmurugan, and M.V. Mirkin, *Anal. Chem* , 2012. **84**(12): p. 5192-5197.

219. Yu, Y., T. Sun, and M.V. Mirkin, *Anal. Chem* , 2016. **88**(23): p. 11758-11766.

220. Marken, F. and J.D. Wadhawan, *Acc Chem Res* , 2019. **52**(12): p. 3325-3338.

221. Bak, E., M. Donten, and Z. Stojek, *Electrochem Commun* , 2005. **7**(5): p. 483-489.

222. Walker, D.S. and G.L. Richmond, *J Am Chem Soc* , 2007. **129**(30): p. 9446-9451.

223. Terry Weatherly, C.K., et al., *J Am Chem Soc* , 2019. **141**(45): p. 18091-18098.

224. Bard, A.J., et al., *Anal. Chem* , 1989. **61**(2): p. 132-138.

225. Ebejer, N., et al., *Anal. Chem* , 2010. **82**(22): p. 9141-9145.

226. Bentley, C.L., M. Kang, and P.R. Unwin, *J Am Chem Soc* , 2017. **139**(46): p. 16813-16821.

227. Güell, A.G., et al., *Proc Natl Acad Sci U S A* , 2012. **109**(29): p. 11487-11492.

228. Mariano, R.G., et al., *Science*, 2017. **358**(6367): p. 1187-1192.

229. Liu, T., et al., *ACS Nano*, 2019. **13**(6): p. 6279-6286.

230. Ying, Y.L., et al., *J Am Chem Soc* , 2018. **140**(16): p. 5385-5392.

231. Hu, K., et al., *J Am Chem Soc* , 2019. **141**(11): p. 4564-4568.

232. Pan, R., et al., *Proc Natl Acad Sci U S A* , 2018. **115**(16): p. 4087-4092.

233. Ivanov, A.P., et al., *ACS Nano*, 2015. **9**(4): p. 3587-3595.

Table of Contents graphic